Review of Aeronautical Fatigue Investigations in Brazil

International Committee on Aeronautical Fatigue and Structural Integrity - ICAF 2025

Prepared by:

Carlos E. Chaves

On behalf of:

Fatigue, Fracture and Structural Integrity Committee

The Brazilian Society of Mechanical Sciences and Engineering (ABCM)

15/3/2025

SUMMARY

This report presents the review of fatigue, fracture and structural integrity investigations performed in Brazil and related to aeronautical structures, from the middle of 2023 to the middle of 2025. Its contents will be made available for public domain by occasion of the 39th ICAF (International Committee on Aeronautical Fatigue and Structural Integrity) Conference to be held in Xi'an, China, in June 09-13, 2025.

CONTENTS

ABBREVIATIONS

ANN	Artificial Neural Network
ABCM	Brazilian Society of Engineering and Mechanical Sciences
ADPR	Average Driving Point Residue
AISI	American Iron and Steel Institute
ALS	Airworthiness Limitation Section
ANAC	Agência Nacional de Aviação Civil (National Civil Aviation Agency of Brazil)
ANN	Artificial Neural Network
ASTM	American Society of Testing and Materials
BEFM	Beam on Elastic Foundation Model
CBBM	Compliance-Based Beam Model
CBT	Corrected Beam Theory
CCM	Compliance Calibration Method
CDM	Continuum Damage Mechanics
CFR	Code of Federal Regulations
CFRP	Carbon Fiber Reinforced Plastics
CIE	Charpy Impact Energy
CLSM	Confocal Laser Scanning Microscopy
CN	Chevron Notch (Test)
CZM	Cohesive Zone Model
DCB	Double Cantilever Beam
DCM	Displacement Correlation Method
DIC	Digital Image Correlation
DoE	Design of Experiments
DSLR	Digital Single-Lens Reflex
EASA	European Aviation Safety Agency
EI	Effective Independence
EVP	Eigenvector Product
FAA	Federal Aviation Administration
FE	Finite Element
FEA	Finite Element Analysis
FEM	Finite Element Method

FF	Fretting Fatigue
FFM	Finite Fracture Mechanics
FIM	Fisher Information Matrix
FRF	Frequency Response Function
FT	Fourier Transformation
GFEM	Generalized Finite Element Method
HE	High Energy
HLU	Hand Lay-Up
ICA	Independent Component Analysis
ICA	Instructions of Continued Airworthiness
IE	Information Entropy
IOM	Injection Overmolding
ITA	Aeronautics Institute of Technology
KE	Kinetic Energy
LA	Lichtenberg Algorithm
LDR	Local Defect Resonance
LEFM	Linear Elastic Fracture Mechanics
LIB	Lithium-Ion Battery
LLT	Low Load Transfer (Specimen)
LOV	Limit of Validity
MAF	Modified Arcan Fixture
MOLA	Multi-Objective Lichtenberg Algorithm
MBT	Modified Beam Theory
MDCD	Main Deck Cargo Door
ML	Machine Learning
MRH	Maximum Rectangular Hull (Method)
MWCM	Modified Wöhler Curve Method
NN	Neural Network
OMA	Operational Modal Analysis
PC	Polycarbonate
PCA	Principal Component Analysis
PMPE	Principle of Minimum Potential Energy
PSD	Power Spectrum Density
R&D	Research and Development

SA	Semi-Analytical (Model)
SBT	Simple Beam Theory
SERR	Strain Energy Release Rate
SGFEM	Stable Generalized Finite Element Method
SEM	Scanning Electron Microscopy
SHM	Structural Health Monitoring
SIF	Stress Intensity Factor
SPO	Sensor Placement Optimization
SSB	Solid-state Sodium-Based Battery
SWT	Smith-Watson-Topper
TAI	Tensile After Impact
TBT	Timoshenko Beam Theory
TCD	Theory of Critical Distances
TCH	Type Certificate Holder
TOPSIS	Technique for Order of Preference by Similarity to Ideal Solution
ULSF	Ultimate Lap-Shear Force
UnB	Federal University of Brasília
UNIFEI	Federal University of Itajubá
USP	University of São Paulo
WFD	Widespread Fatigue Damage

SYMBOLS

da/dN	Crack propagation rate (for metallic materials)
dL/dN	Crack propagation rate (for composite materials)
G_{max}	Maximum strain energy release rate
K_{Ic}	Plane strain fracture toughness
ΔK	Stress intensity factor variation
$\sigma_{p,max}$	Maximum principal stress
$\sigma_{p,min}$	Minimum principal stress
$\sigma_{p,a}$	Principal stress amplitude
$\sigma_{n,max}$	Maximum normal stress
σ_{r}	Remote stress
τ_{a}	Shear stress amplitude
σ_{w}	Fatigue strength for materials with micro defects

LIST OF FIGURES

1. INTRODUCTION

The present document is a summary of fatigue investigations related to aerospace materials and structures performed by Brazilian organizations (or by Brazilian researchers) over the past two years. The complete document will be made available on-line (via icaf.aero website) by occasion of the 39th ICAF (International Committee on Aeronautical Fatigue and Structural Integrity) Conference to be held in Xi'an, China, between June 09th and June 13th, 2025.

Some of the research works presented along this review are follow on research activities related to the ones previously presented in previous National Reviews.

The following are the main Brazilian institutions that have collaborated during this period with research works on fatigue and fracture mechanics related to aeronautical products, and had scientific or technological research works added to this review:

- Brazilian Society of Engineering and Mechanical Sciences (ABCM) – Rio de Janeiro – RJ
- University of São Paulo (USP) – São Carlos – SP
- University of São Paulo (USP) – Lorena - SP
- Federal University of Brasília (UnB) – Brasília - DF
- Federal University of Itajubá (UNIFEI) – Itajubá – MG
- Federal University of São Carlos (UFSCar) – São Carlos – SP
- Federal University of São Paulo (UNIFESP) – São José dos Campos - SP
- Aeronautics Institute of Technology (ITA) – São José dos Campos – SP
- Embraer S/A – São José dos Campos – SP

Further, some works to be presented were developed in cooperation with foreign institutions, from which some are mentioned here:

- University of Porto (U.Porto) - Portugal
- Technical University of Graz (TU-Graz) - Austria

As for the previous years, the author of this report would like to thank all partners from the academy and the research institutes that have collaborated with this compilation, and that will be cited along with the report. The author is grateful to Professors Mariano Andrés Arbelo and Maurício Vicente Donadon, from the Aeronautics Institute of Technology (ITA), Professor Volnei Tita and Professor Carlos Baptista, from the University of São Paulo (USP), Professor Guilherme Ferreira Gomes, from Federal University of Itajubá (UNIFEI), , Professor José Alexander Araújo, from the University of Brasília (UnB), Professor Mirabel

Rezende (UNIFESP), Dr. Willy Mendonça, Mr. Paulo Pasquali and Mr. Wagner Rissardo from Embraer S/A, and many others, for their continuous support in current activities related to fatigue, fracture and structural integrity in aerospace structures and materials. Finally, the author would like to thank Ms. Carolina Maekawa, who helped with the compilation of articles and organization of the report.

The following are highlights from this report, organized according to the topics:

Crack Growth Analysis and Simulation

- Utilization of the Stable Generalized Finite Element Method (SGFEM) for analyzing crack propagation due to fatigue.
- SGFEM provides accurate stress intensity factor values and fatigue life estimates, surpassing traditional methods like the Generalized Finite Element Method (GFEM).

Metallic Materials and Structures

- Development of marker bands for accurately tracking crack propagation in shear joints.
- Use of Artificial Neural Networks (ANN) and simple linear regression strategies for estimating fretting fatigue lives.
- Investigation into the influence of interrupted aging (T6I4) on the hardness and fracture toughness of AA7050 alloy.

Composite Materials and Structures

- Numerical and experimental studies on using fasteners to arrest delamination in composite laminates under Mode I loading.
- Finite Fracture Mechanics (FFM) model applied to fatigue damage growth in CFRP laminates, with a focus on fiber orientation effects.
- Impact damage and subsequent tensile fatigue behavior analyzed in CFRP laminates.

Hybrid Structures

- Study of mechanical durability and hygrothermal stability of polycarbonate and aluminum alloy AA6061 hybrid joints produced via injection overmolding.

Structural Health Monitoring

- Evaluation of all-solid-state sodium-based batteries as potential strain-sensing devices under vibrational loads.
- Multi-objective Kriging-based approach for sensor placement optimization in composite aircraft structures.

Airworthiness

- Embraer's compliance with FAA's Widespread Fatigue Damage (WFD) Rule and EASA's Part 26 Ageing Aircraft Requirements.

All papers, dissertations, theses and conference proceedings presented in this document were directly supplied by their authors, co-authors and advisors to the author of this review, and a number of these works were previously presented in conferences or published in technical journals or are available from public sources.

2. CRACK GROWTH ANALYSIS AND SIMULATION

Analysis of crack propagation due to fatigue using the Stable Generalized Finite Element Method (SGFEM) (ITA - Ref. [1][2])

Summary:

This work investigates the integration of the Stable Generalized Finite Element Method (SGFEM) and the Displacement Correlation Method (DCM) for analyzing two-dimensional crack propagation problems caused by fatigue. Traditional Finite Element Method (FEM) approaches often require excessive mesh refinement, especially near crack tips, to achieve accurate results, which can be computationally expensive. The SGFEM overcomes this challenge by utilizing enrichment functions to create a global approximation space without requiring mesh-to-crack alignment, while maintaining numerical stability and conditioning.

DCM is chosen for Stress Intensity Factor (SIF) extraction due to its computational efficiency and simplicity compared to energy-based methods like J integral. The method's accuracy is further enhanced through a linear least squares extrapolation technique. The study employs the maximum circumferential tension criterion to determine crack propagation direction and leverages well-established propagation laws to analyze crack growth under cyclic loading conditions.

The study concludes that the SGFEM, combined with DCM, offers a robust and efficient solution for analyzing fatigue-induced crack propagation. It consistently delivers more accurate SIF values and fatigue life estimates compared to GFEM. The authors suggest further improvements to the SGFEM formulation to enhance stability and convergence.

Highlights:

Two numerical examples are provided to validate the proposed approach. The first example (Figure 1) examines an aluminum plate with a central hole and an initial edge crack, subjected to cyclic uniaxial loading. The SGFEM's SIF values are found to be more accurate than those obtained using the Generalized Finite Element Method (GFEM), with relative errors consistently below 5%. Additionally, the estimated number of cycles to failure using SGFEM closely matches the reference solution provided by NASGRO®, a widely adopted commercial software in the aeronautics industry.

The second example (Figure 2) involves an aluminum rectangular plate with two holes and inclined initial cracks, also under cyclic uniaxial loading. The crack paths predicted by SGFEM are compared to experimental data and exhibit a similar trend, validating the method's accuracy. SGFEM’s SIF values lead to crack propagation rates that closely align with experimental observations, whereas GFEM results tend to be less conservative.

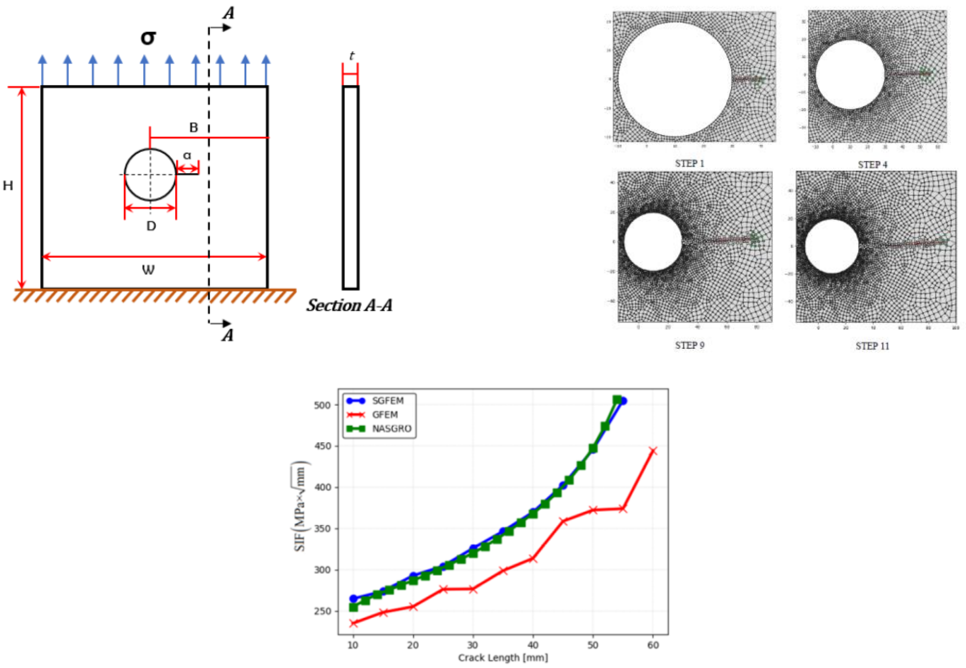

Figure 1 – First example: plate with a hole edge crack. Top: geometry and boundary conditions. Center: selected crack propagation steps. Bottom: SIF results comparison (SGFEM, GFEM and NASGRO).

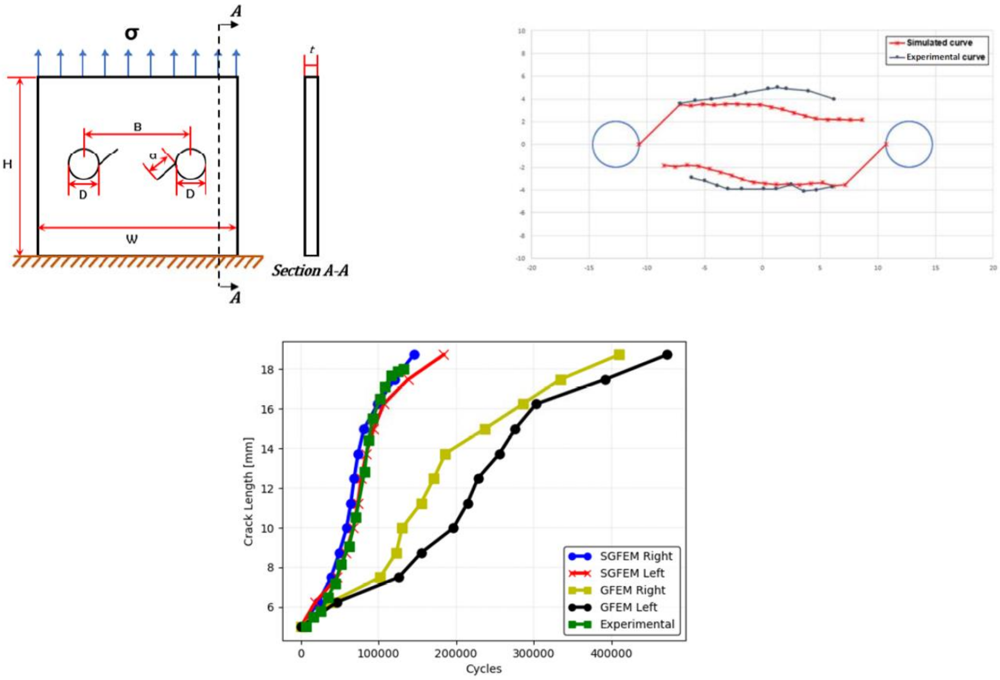

Figure 2 – Second example: plate with two holes and inclined initial cracks. Top: geometry and boundary conditions. Bottom: crack path comparison (simulation vs. experimental). Right: crack propagation curves (SGFEM, GFEM and experimental).

3. METALLIC MATERIALS AND STRUCTURES

Fatigue and Fracture Properties

Development of a marker band code for different da/dN rates (Embraer)

Summary:

The structural integrity of shear joints is critical in various engineering applications, where the ability to accurately predict and monitor crack propagation is essential to ensure safety and performance. A groundbreaking project was undertaken to develop a Marker Band code for different da/dN rates in shear joints with low load transfer.

Figure 3 shows a typical low load transfer (LLT) shear joint specimen used in the test matrix development.

Figure 3 – Low load transfer (LLT) specimen.

The marker bands enable the generation of the crack propagation curve a(mm) vs N(cycles) since their initiation with precision, which is not possible with the usual inspection methods (visual, edge current, ultrasound, etc.), because in the initial stages of crack propagation it is too small to be identified by such methods.

The main challenge in this technique is to develop a marker band code that can be easily identified whether it is close to or far from fatigue initiation.

The use of marker bands dates back to the 1970s and is gaining new momentum for applications that seek a greater understanding of complex scenarios for damage tolerance.

Figure 4 shows the same marker bands with the same magnification in different regions of the damage surface. The marker bands move away with the evolution of crack propagation. Ideally, each marker band should have a code that allows its correlation with the cycles of the applied spectrum, thus making it possible to make the correlation more quickly and efficiently and also observe the interaction among different crack fronts.

Figure 5 shows the correlation between the load spectrum and the marker bands.

This activity is being carried out by the Embraer R&D Department.

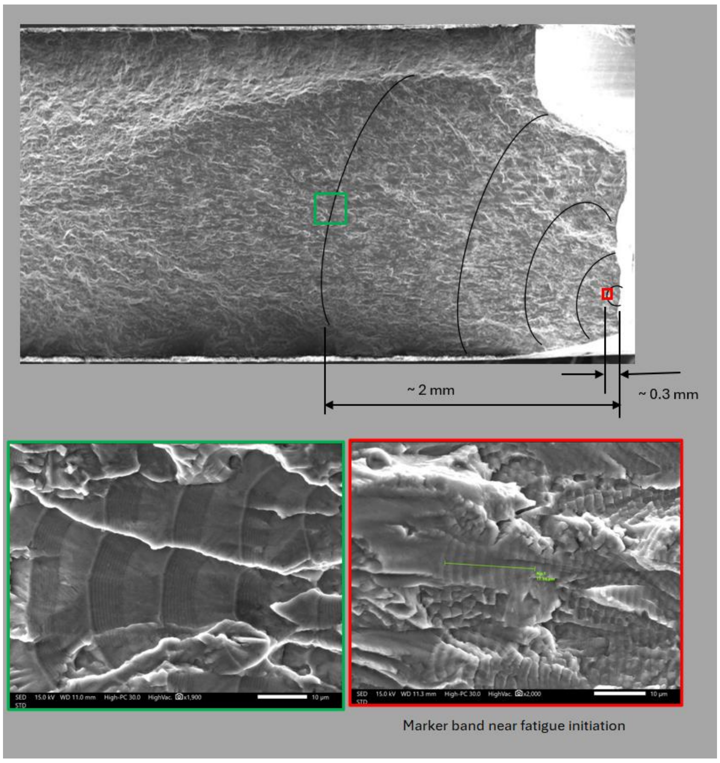

Marker band near fatigue initiation

Figure 4 - Different aspects of the marker bands.

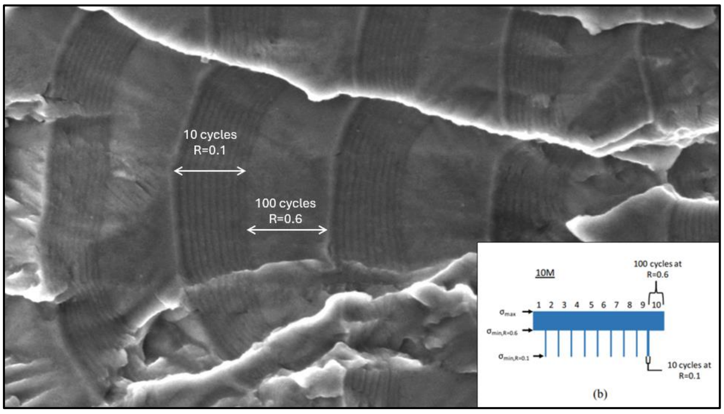

Figure 5 – Example of a detail with marker bands.

Fretting Fatigue

A simple linear regression strategy for fretting fatigue life estimates (UnB - Ref. [3])

Summary:

Recently, an increasing amount of works have been considering the use of Machine Learning (ML) approaches to tackle the fretting fatigue problem. Notably, Artificial Neural Networks (ANN) models have been the most widely used ones. In this work, the authors propose a simple linear regression strategy to estimate fretting fatigue lives with a level of accuracy similar to that of more elaborate ML models. Such a simplification is possible by the judicious choice of the input parameters believed to govern the problem investigated. A fair amount of fretting fatigue data collected from the literature was used to test and validate the proposed methodology (206 tests). Life estimates by considering ANN models and a critical plane multiaxial fatigue criterion were used for the sake of comparison. Results have shown that, in terms of life estimates, the linear regression model here presented, in general, performed better than the multiaxial fatigue parameter considered and had an accuracy similar to that of the ANN models. The proposed regression model also provided accurate life estimates for challenging test conditions quite different from those used in its calibration. Moreover, compared to the ANN models, the linear regression one is considerably easier to implement, to train, and it allows an easier physical interpretation of the results.

Highlights:

Fretting fatigue (FF) is a phenomenon that occurs due to micro-slip between contacting surfaces under cyclic loading, leading to premature failure in critical components such as aeronautical engines, bolted joints, and power cables. Various approaches have been developed to estimate FF life, including continuum damage mechanics and crack propagation models. Recently, machine learning techniques, particularly artificial neural networks (ANNs), have been explored for FF life predictions.

FF involves multiaxial and non-proportional stress states, making fatigue assessment complex. Critical plane models such as the Modified Wöhler Curve Method (MWCM) define a plane experiencing the highest shear stress amplitude and maximum normal stress. These parameters are essential for predicting FF life. The study incorporates the Theory of Critical Distances (TCD) to account for strong stress gradients, ensuring accurate nonlocal stress evaluation.

A dataset of 206 FF tests from the literature, covering aluminum alloys and titanium alloys, was used to develop and validate the model. The tests were conducted under partial slip conditions with different contact geometries.

Additionally, challenging FF scenarios, including cyclic normal contact loads and elevated temperatures, were considered to test the model's generalization capabilities. Figure 6 shows the schematic of the FF model.

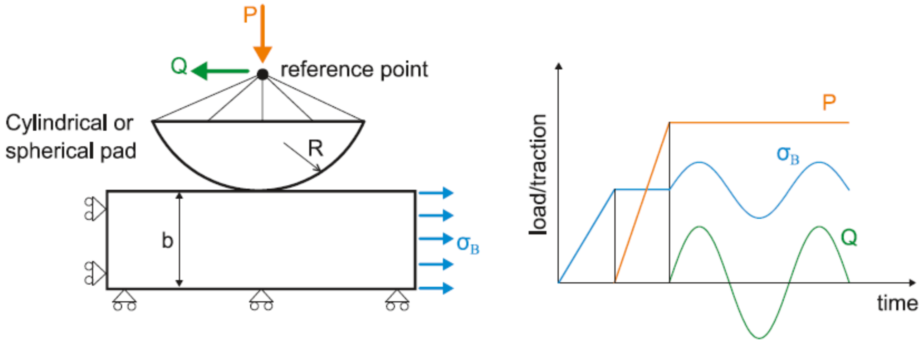

Figure 6 - Schematic representation of the fretting fatigue model.

Finite element (FE) simulations were employed to compute the necessary stress parameters for FF life estimation. The models accounted for variations in material properties, loading conditions, and stress gradients. The shear stress and the maximum normal stress (according to the MWCM definition) were computed at a point L/2 distant from the right-side contact edge (the region where crack initiation is commonly observed). Figure 7 shows τ_a and $\sigma_{n,max}$ vs. fatigue life. These results were further used to calibrate the linear regression models.

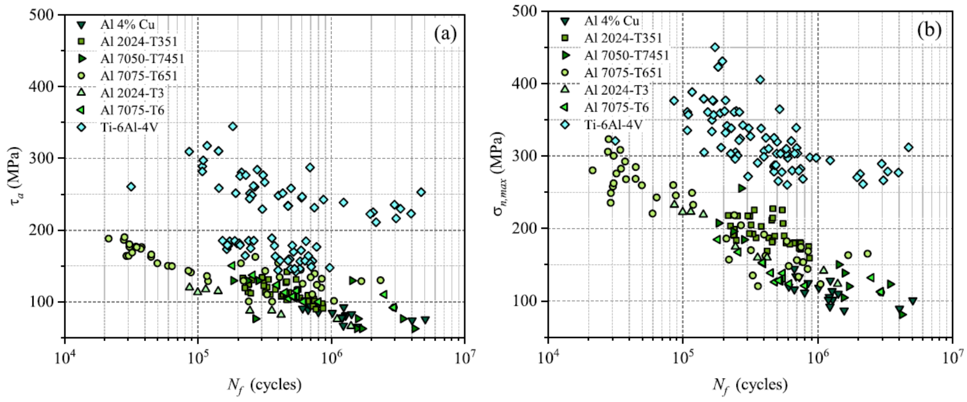

Figure 7 - MWCM multiaxial stress parameters for the FF data investigated: (a) shear stress amplitude vs. life and (b) maximum normal stress vs. life.

Two linear regression models were developed: RM1 and RM2. Both used three input parameters: the shear stress amplitude, the maximum normal stress (with RM2 incorporating a squared term), and the material yield strength, all normalized by the ultimate strength. The output variable was the logarithm of fatigue life. Model coefficients were determined through least-squares minimization.

The proposed regression models were tested against ANN-based predictions and the MWCM fatigue criterion. RM1 demonstrated better performance than MWCM and comparable accuracy to ANN models while requiring significantly fewer computational resources. RM1 also provided accurate life estimates under challenging conditions, including cyclic contact loads and elevated temperatures. Sensitivity analysis showed that the model performed well even with limited training data. Figure 8 shows the model performance comparison.

This study presents a simple yet effective linear regression model for FF life estimation. The model offers similar accuracy to ANN-based approaches but with easier implementation and interpretation. It also demonstrates strong generalization capabilities across various materials and loading conditions. The findings suggest that linear regression can be a viable alternative to more complex machine learning models in FF life prediction.

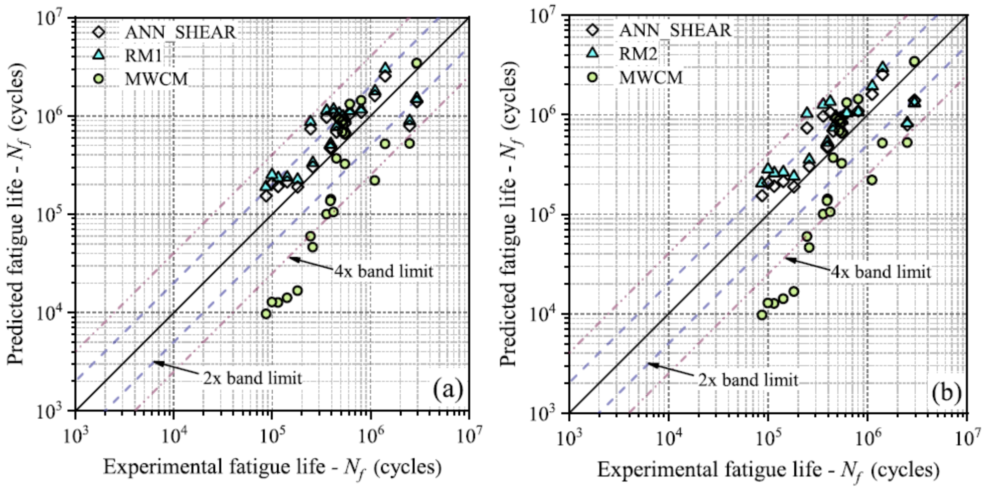

Figure 8 - Life estimates for the Al testing data: (a) RM1 model and (b) RM2 model.

A new multiaxial fatigue endurance model for high strength steels taking into account the presence of small defects (UnB - Ref. [4])

Summary:

In this work, a new multiaxial fatigue model is proposed for metallic material with small defects. This model correlates the uniaxial fatigue limit obtained from the $\sqrt{area}$ parameter of a high strength steel containing small defect with values associated with the amplitude of the principal stresses, whose calculation for non-proportional loadings is not trivial. The performance of the model was evaluated with experimental data from AISI 4140 steel, under various loading conditions, in which smooth cylindrical bars were considered, regarding: (i) the effect of non-metallic inclusions in the material, and (ii) superficial micro hole with a straight bottom machined in the material (550 μm in diameter and depth). The proposed model has provided accurate fatigue strength estimates with average error not exceeding 16%.

Highlights:

The presence of small defects significantly influences the fatigue strength of high-strength steels. Various models, including Murakami's $\sqrt{area}$ parameter, have been developed to estimate fatigue limits under uniaxial loading. However, real-world components often experience multiaxial stress states. This study proposes a new model that extends existing fatigue endurance models by incorporating principal stress amplitude calculations for multiaxial conditions.

Murakami's model estimates fatigue limits based on the defect size and Vickers hardness (Hv), expressed as: $\sigma_w = 1.43(Hv + 120)\left(\sqrt{area}\right)^{-\frac{1}{6}}$ for surface defects and $\sigma_w = 1.41(Hv + 120)\left(\sqrt{area}_{max}\right)^{-\frac{1}{6}}$ for internal defects. The upper limit for $\sqrt{area}$ applicability is approximately 1000 μm. The study adapts this approach to multiaxial stress conditions.

The new model introduces a modified Smith-Watson-Topper (SWT) parameter: $SWT_{mod} = \sqrt{\sigma_{p,max} \cdot \sigma_{p,a}}$ where $\sigma_{p,max}$ is the maximum principal stress and $\sigma_{p,a}$ is the principal stress amplitude. Unlike previous models, this approach accounts for varying principal stress directions under non-proportional loading. The Maximum Rectangular Hull (MRH) method was employed to calculate principal stress amplitudes, accommodating complex stress paths. Figure 9 illustrates principal stress variations under different loading conditions.

The study utilized AISI 4140 steel. Two specimen types were tested: smooth cylindrical bars and those containing a 550 μm micro-hole (Figure 10). The specimens were machined and polished following ASTM E466-15 standards. Experiments were conducted using servo-hydraulic fatigue testing machines (Figure 10) under different loading conditions: uniaxial, in-phase, and 90° out-of-phase combined loading. Failure criteria were set at 2 × 10^6 cycles, with stress levels adjusted iteratively.

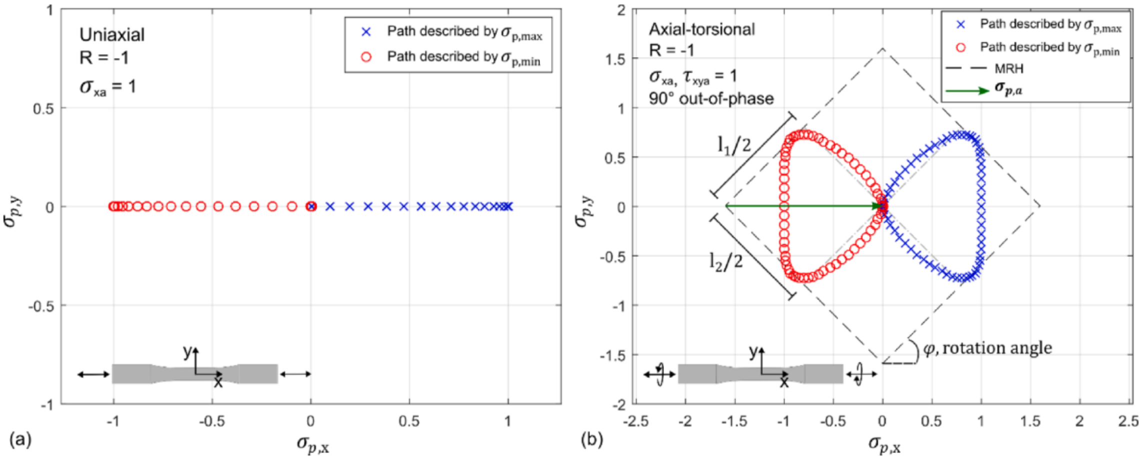

Figure 9 - Path described by the principal stresses in two loading conditions: (a) traction-compression and (b) combined out-of-phase loading with application of the MRH to calculate $\sigma_{p,a}$.

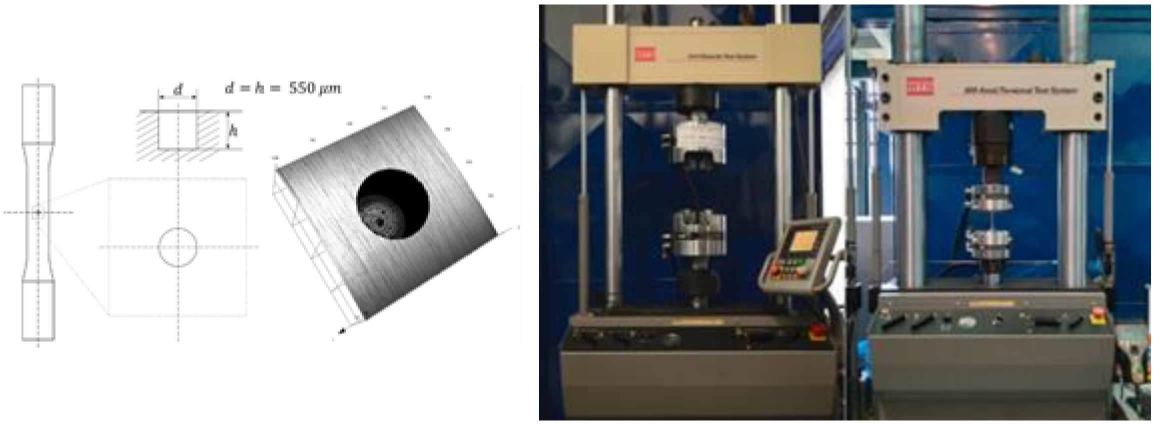

Figure 10 - On the left, micro hole produced in fatigue specimens. On the right, Fatigue Testing Machines, MTS - 810 Material test system and MTS - 809 Axial/torsional test system.

Fatigue limits were calculated for specimens with natural inclusions ($\sqrt{area}_{max} = 145\ \mu m, \sigma_w = 271\ MPa$) and micro-holes ($\sqrt{area} = 550\ \mu m, \sigma_w = 220\ MPa$), showing a 19% reduction in endurance. Experimental results aligned well with model predictions. Smooth specimens exhibited conservative predictions, particularly under in-phase loading. Micro-hole specimens showed minimal error (Figure 11), confirming the model's reliability in accounting for defect-induced fatigue behavior. Error indices ranged from 9.86% to 26.41%, with a maximum error of 43.91%. The model's slightly conservative nature ensures safer engineering applications. Long-term testing (10^7 cycles) indicated an endurance limit beyond 2×10^6 cycles, validating the stopping criterion.

The proposed multiaxial fatigue model effectively incorporates the influence of small defects using the $\sqrt{area}$ parameter and a modified SWT approach. The method requires no additional material constants and offers a practical alternative for fatigue strength estimation without extensive experimental testing. The results demonstrate its applicability in engineering scenarios where multiaxial stress states and small defects coexist.

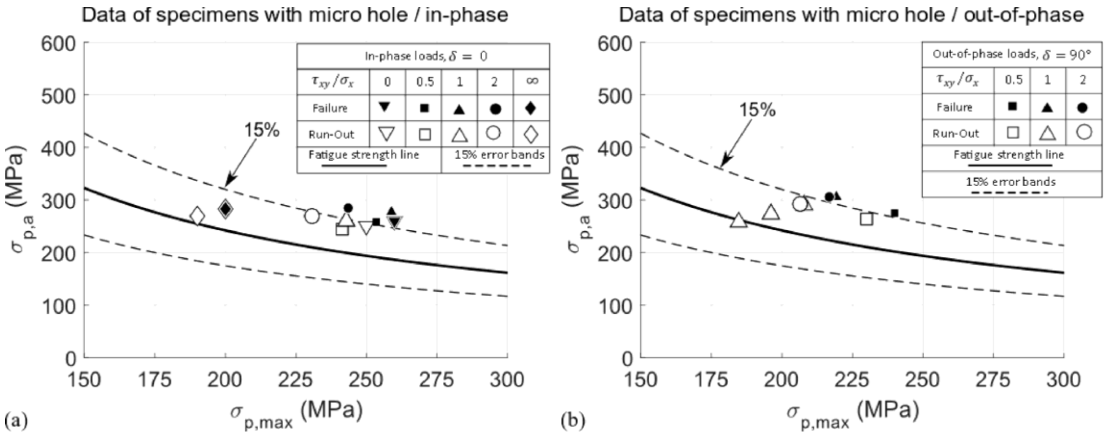

Figure 11 - SWT$_{mod}$ prediction and experimental data of specimens with a micro hole, (a) uniaxial and combined in-phase and (b) combined out-of-phase data.

On the generalization capability of artificial neural networks used to estimate fretting fatigue life (UnB - Ref. [5])

Summary:

This study assesses the generalization capacity of artificial neural networks (ANNs) for predicting fretting fatigue of mechanical contacts using different materials and geometries. These ANN utilize as inputs, material properties and stress quantities that have been physically related to the fatigue crack initiation mechanism under multiaxial loading. Initially trained and validated on aeronautical aluminum alloys data, one tests their generalization performance by applying them to fretting fatigue data for Ti-6Al-4V, ASTM A743 CA6NM steel, and Al 7050- T745, employing both cylindrical and spherical pads under various loading conditions, including out-of-phase loading. The ANNs adeptly predict fatigue lives across this extensive dataset, surpassing classical multiaxial fatigue criteria in accuracy. This underscores the effectiveness of ANN-based methodologies in diverse fretting fatigue scenarios.

Highlights:

Fretting fatigue (FF) is a critical issue in mechanical assemblies, leading to premature failure due to high-stress gradients at contact surfaces. This phenomenon occurs under cyclic loading and small relative slip between contacting components, inducing complex multiaxial stress states. Traditional models for predicting FF life include analytical approaches such as the Smith, Watson, and Topper (SWT) model, the Modified Wöhler Curve Method (MWCM), and the Crossland criterion. However, these models often require extensive material-specific calibration. Artificial Neural Networks (ANNs) have emerged as a promising alternative for FF life prediction due to their ability to learn from experimental data and generalize across different materials and loading conditions.

This study assesses the performance of three ANN models trained on aeronautical aluminum alloys and tested on other materials, including Ti-6Al-4V and ASTM A743 CA6NM steel. The ANNs take as input various stress-related parameters derived from classical multiaxial fatigue models. The study incorporates both cylindrical and spherical contact pad geometries under varying loading conditions, including out-of-phase effects. The ANN models utilized a feedforward architecture with one hidden layer and were trained using a backpropagation algorithm based on gradient descent. Figure 12 illustrates the ANN architecture, consisting of an input layer, a single hidden layer with activation functions, and an output layer predicting fatigue life. The training process included cross-validation to prevent overfitting and optimizing generalization capabilities. Figure 12 also shows the modelling process considered in the study.

The ANN models (SHEAR, NORMAL, and INV) were evaluated against experimental FF data and classical fatigue models. The results showed that ANN-based predictions closely matched experimental fatigue life values, outperforming traditional models, especially under out-of-phase loading conditions. The SHEAR and INV models provided the best predictions, demonstrating lower error margins compared to the NORMAL model.

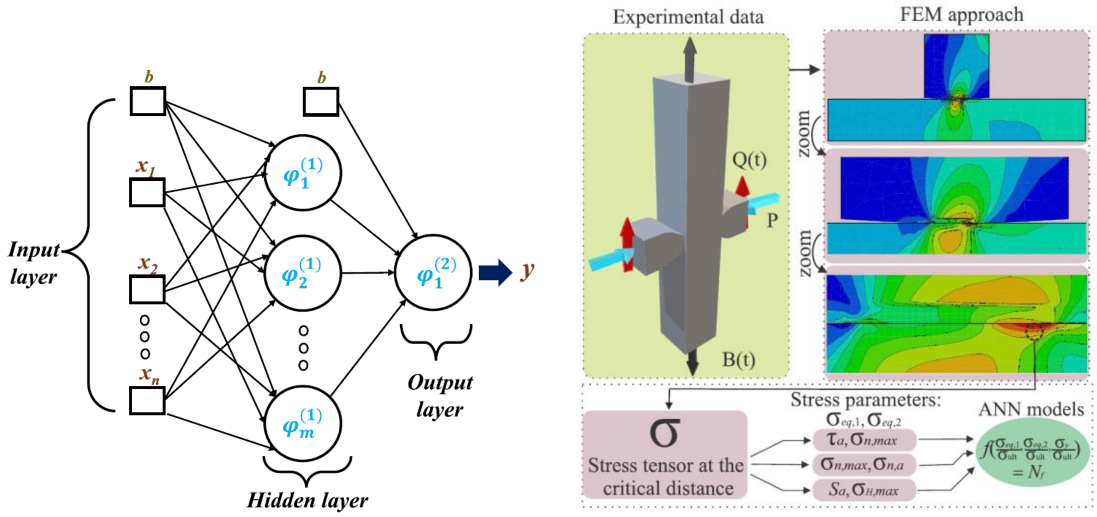

Figure 12 - On the left, example of a simple-layered ANN architecture. On the right, summary of the considered model.

Figure 13 presents the estimated fatigue life versus experimental values for both aluminum and steel alloys. The ANN models exhibited a higher accuracy range compared to classical models, indicating their superior generalization ability. Additionally, Figure 14 compares ANN predictions with experimental results, reinforcing the models' reliability.

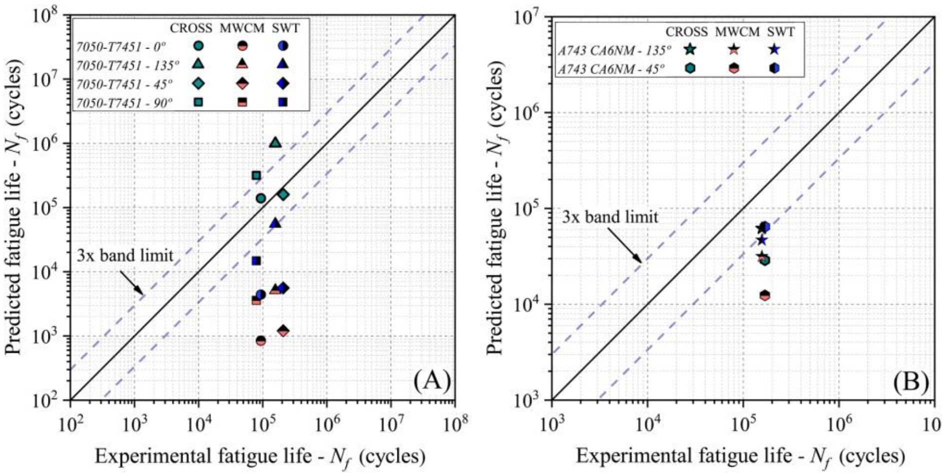

Figure 13 - Estimated fatigue life considering all the multiaxial fatigue models vs. experimental one for the Al 7050-T7451 alloy (A), and ASTM A743 CA6NM alloy (B).

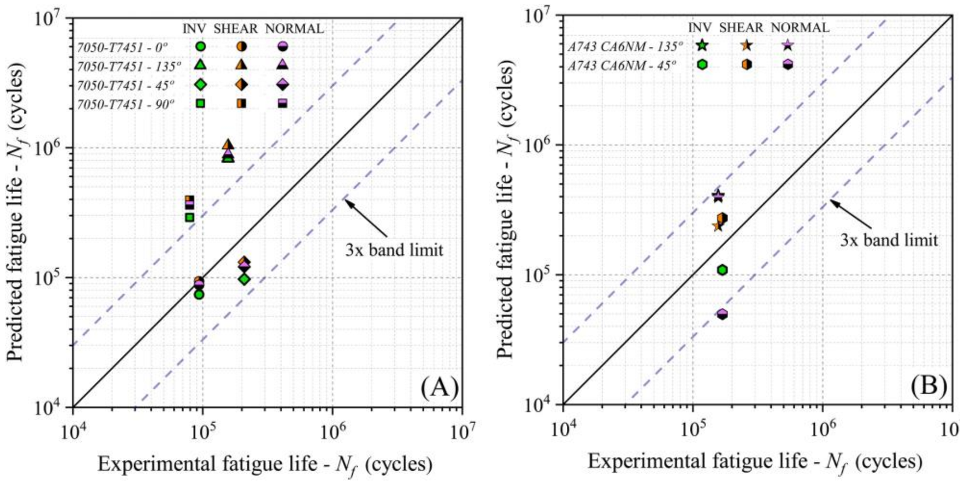

Figure 14 - Estimated fatigue life considering all the ANN models vs. experimental one for the Al 7050-T7451 alloy (A), and ASTM A743 CA6NM alloy (B).

A key advantage of the ANN models is their ability to predict fatigue life without requiring recalibration for different materials, a limitation commonly faced by traditional fatigue criteria. This highlights the robustness of ANNs in handling varying stress conditions and material properties.

This study demonstrated the strong generalization capability of ANN models for fretting fatigue life prediction across different materials and loading scenarios. The

ANN models significantly outperformed classical multiaxial fatigue models, providing accurate predictions without requiring additional material-specific calibration. Among the models analyzed, the SHEAR and INV approaches yielded the most precise estimates, confirming the relevance of shear and invariant stress parameters in fatigue life assessments. Future work may focus on expanding datasets and exploring deeper neural network architectures to further enhance predictive accuracy.

A Generalized ANN-Multiaxial Fatigue Nonlocal Approach to Compute Fretting Fatigue Life for Aeronautical Al Alloys (UnB - Ref. [6])

Summary:

Fretting fatigue (FF) occurs when contacting parts experience small amplitude relative slip and fatigue loads. This phenomenon is prevalent in aeronautical applications such as turbine blade/disc joints and electrical conductors, often leading to premature crack initiation and failure. Traditional methods for estimating fretting fatigue life include nonlocal stress models, linear elastic fracture mechanics (LEFM), and continuum damage mechanics (CDM). However, these approaches require complex material calibrations. This study proposes an alternative methodology that integrates artificial neural networks (ANNs) with non-local stress parameters to improve FF life predictions for aluminum alloys used in aerospace applications.

The study introduces two ANN models trained on fretting fatigue data from various Al alloys. These models incorporate nonlocal stress parameters as input features, specifically the Modified Wöhler Curve Method (MWCM) and the Smith, Watson, and Topper (SWT) model. The MWCM Model evaluates fatigue damage based on the plane where the maximum shear stress amplitude occurs while considering the role of normal stresses. The SWT Model uses the product of the maximum normal stress and strain amplitude on the critical plane for fatigue assessment.

The inputs for the ANN models include equivalent stress parameters, normalized by material properties (yield stress and ultimate tensile strength), and calculated at a material-dependent critical distance.

Highlights:

The models were trained on experimental FF data from six different Al alloys under various contact conditions (cylindrical and spherical contacts) and stress regimes.

To validate the ANN approach, fretting fatigue experiments were gathered from literature sources covering six Al alloys: Al 4%Cu, 2024-T351, 7050-T7451, 7075-

T651, 2024-T3, and 7075-T6. These experiments involved different geometries (cylinder-on-flat and sphere-on-flat configurations) and a broad range of applied loads. Finite element simulations (ABAQUS) were used to determine the stress distributions in the FF contact regions.

For training and validation:

- The dataset was split into training (99 data points) and testing (9 data points), while query data (24 additional cases) were used to evaluate model generalization.

- The ANN architectures were optimized using backpropagation with the Xavier weight initialization method and a tangent hyperbolic activation function.

- Model outputs were normalized fatigue life predictions in logarithmic scale.

Both ANN models (ANN_SHEAR and ANN_NORMAL) significantly outperformed traditional multiaxial fatigue models (MWCM and SWT) in estimating FF life.

The ANN models provided estimates within a factor of two from experimental results, demonstrating strong generalization across different alloys, geometries, and loading conditions. The Empirical risk error (ER) was calculated for each model, showing that ANN models reduced prediction errors by over 70% compared to traditional methods. The ANN_NORMAL model performed better for the 2024-T3 alloy, while the ANN_SHEAR model was more effective for 7075-T6 alloy, aligning with material-dependent crack initiation mechanisms. Life surfaces plotted for 7075-T651 showed that the ANN models accurately captured the influence of shear and normal stress parameters on fatigue life.

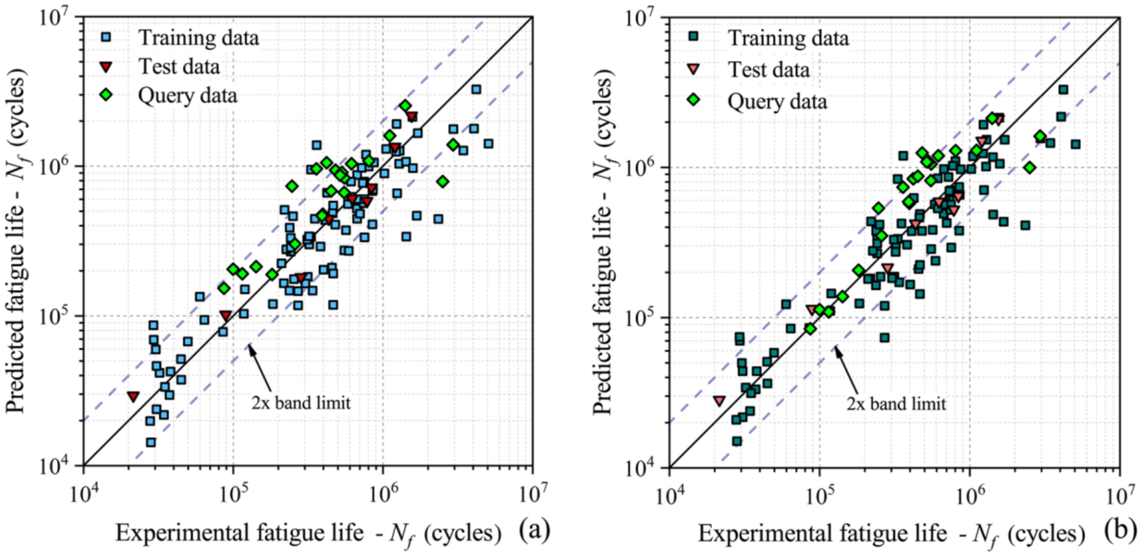

Figure 15 - Estimated fatigue life by the ANN_SHEAR model vs. the experimental one (a). Estimated fatigue life by the ANN_NORMAL model vs. the experimental (b).

The study successfully demonstrates the potential of ANN-based models for predicting fretting fatigue life in aeronautical Al alloys. These models provide improved accuracy, robustness, and ease of use compared to traditional fatigue life estimation methods. Unlike conventional models, ANN approaches do not require material-specific calibrations, making them more suitable for practical engineering applications. Future work will focus on extending the model's generalization to other materials and loading conditions.

Mechanical Processes and Surface Treatments

Effects of interrupted aging T6I4 on hardness and fracture toughness of aeronautic AA7050 alloy (USP - Ref. [7])

Summary:

Al–Zn–Mg–Cu alloys have been extensively researched for aeronautical uses due to their good mechanical properties. Among these alloys, AA7050 is notable for its impressive fracture toughness. Alternative heat treatments have been developed to improve fracture toughness without compromising AA7050 strength. T6I4, a method involving under aging for short times and secondary aging, is one of them. The main objective of this research was to investigate the influence of T6I4 temper on the hardness and fracture toughness of AA7050 alloy. A 75-mm thick plate of AA7050-T7451 alloy was microstructurally characterized in three directions regarding the rolling direction. Nine interrupted aging conditions were statistically evaluated for their Vickers microhardness measurements of the treated samples, from which two of them were chosen for Chevron-notch (CN) tests. Chevron-shaped specimens with L-S orientation were produced from the T7451, T6I4-24, and T6I4-72 conditions. Charpy V-notch impact tests were performed to obtain alternative estimates of the fracture toughness of AA7050 alloy in the T7451 and T6I4-24 states. The results from the CN and Charpy tests indicated that the T6I4-24 temper provides to this alloy a higher capacity to accumulate plastic deformation. Furthermore, the analysis of fracture surfaces of Chevron-shaped specimens suggested that the fracture topography of T6I4-24 samples is more irregular with more ductile features than that of the T7451 and T6I4-72 conditions.

Highlights:

The material studied was a 75-mm thick plate of AA7050-T7451 aluminum alloy. Samples were prepared and subjected to nine different T6I4 conditions, varying the first and second aging stages. Vickers microhardness tests were conducted to determine the optimal secondary aging duration. Chevron-notch tests were performed using L-S oriented specimens to evaluate fracture toughness under three conditions: T7451, T6I4-24, and T6I4-72. Additionally, Charpy V-notch tests were conducted on selected samples to estimate fracture toughness.

The Vickers microhardness measurements showed that the second stage of aging significantly influenced hardness, with the highest values observed for 30 min of first stage aging and 72 h of second-stage aging. Optical microscopy and SEM analyses revealed grain structure differences in the L, T, and S faces, with elongated grains in the rolling direction. Figure 16 shows micrographs of different grain orientations, grain size distribution histograms and SEM images.

The load-CMOD curves for the three conditions (T7451, T6I4-24, and T6I4-72) are illustrated in Figure 17. The T6I4-24 condition demonstrated the highest resistance to crack propagation, attributed to finer, more uniformly distributed strengthening precipitates. Fractographic SEM images revealed that T6I4-24 samples exhibited a more irregular fracture surface with secondary cracks, indicating better plastic deformation capability.

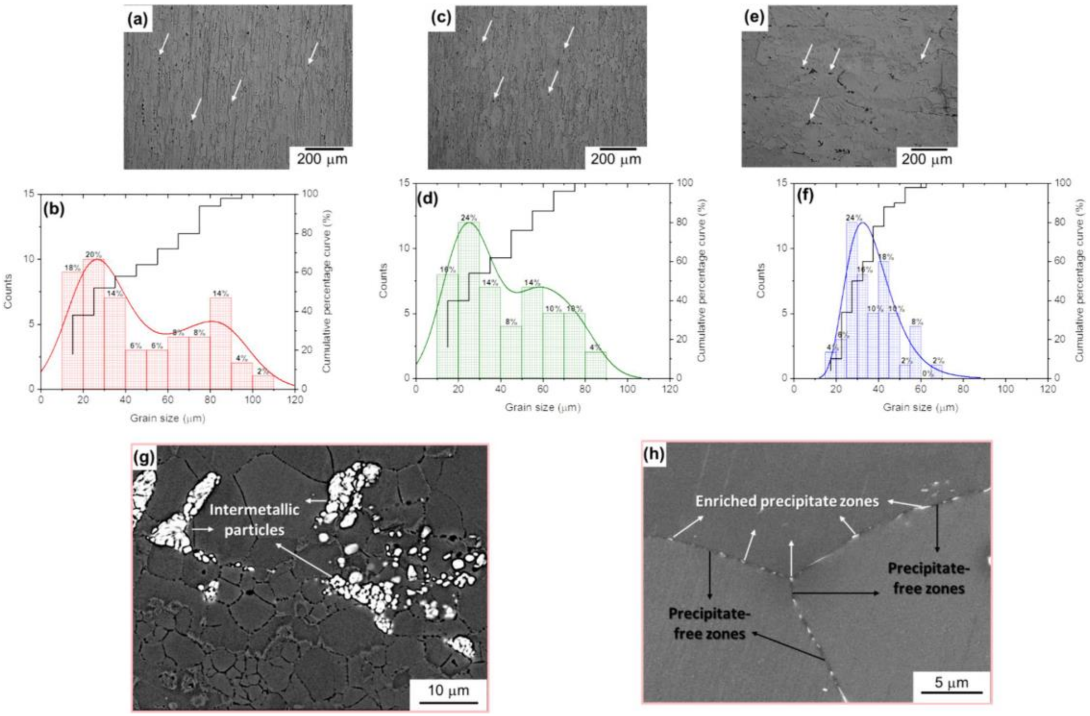

Figure 16 - Optical micrographs and grain size distribution histograms of AA7050-T7451 samples in L (a, b), T (c, d), and S (e, f) faces regarding the rolling direction. SEM images of an AA7050-T7451 sample in the L face with magnifications of (g) 3000X and (h) 20000X.

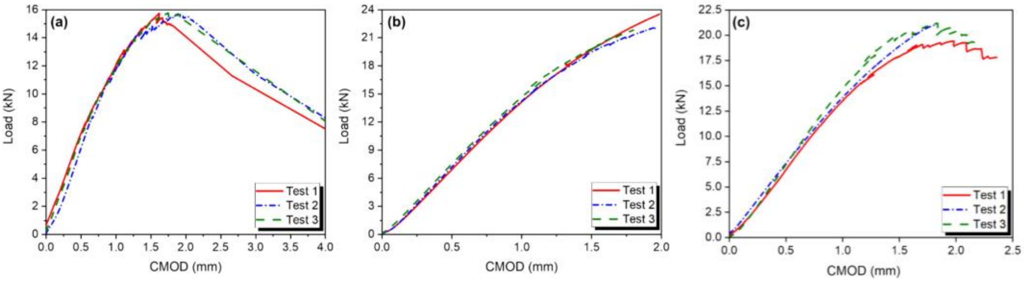

Figure 17 - Load-CMOD curves for AA7050: a T7451, b T6I4-24, and c T6I4-72.

The T6I4-24 condition exhibited significantly higher Charpy impact energy (CIE) compared to T7451, suggesting improved fracture toughness under high deformation rates. The relationship between CIE and K_{Ic} values was examined using three predictive models, with the most accurate results incorporating yield strength considerations.

The statistical analysis of secondary aging demonstrated that prolonged second-stage aging promotes the growth of strengthening precipitates, increasing hardness. The Chevron-notch test results suggest that the T6I4-24 condition provides a balanced combination of strength and toughness, whereas T6I4-72 showed reduced fracture resistance due to precipitate coarsening. The Charpy test findings further support the superior toughness of T6I4-24, validating its suitability for aerospace applications requiring enhanced damage tolerance.

Metallic Structures

E-190 Freighter Development and Certification (Embraer)

The Embraer E-190 Freighter, also known as the E190F, represents a significant advancement in the air cargo industry, addressing the evolving demands of e-commerce and modern trade. The development of the E190F began in May 2022, with the aim of filling a gap in the air cargo market and replacing older, less efficient models. The E190F is designed to meet the needs of rapid deliveries and decentralized operations, which are essential for the growing e-commerce sector.

The E190F made its first flight in April 2024 and debuted publicly at the Farnborough Airshow in July 2024. It has since achieved full certification from the Federal Aviation Administration (FAA), the National Civil Aviation Agency of Brazil (ANAC), and the European Union Aviation Safety Agency (EASA) by February 2025. This certification allows the E190F to operate globally, providing a versatile and efficient solution for air cargo transportation.

While most of the E190F structure keeps the E190 baseline configuration, already certified and in operation for over a decade, some structures were developed for freighter usage, such as the main deck cargo door (MDCD), the deck floor cargo attachments and a few other structural components. Within these structures, there were details requiring new development and certification.

One of these structural details is the latch that locks the MDCD. This structure was tested for durability for over a million cycles, without findings, ensuring that there would be no issue related to fatigue or wearing over the aircraft operational life.

Below, *Figure 18* shows an overview of the E190F, with emphasis on the cargo door and the latch/hook positions. *Figure 19* shows an overview of the latch/hook durability test.

(a)

(b)

Figure 18 - Embraer E190F overview. (a) aircraft, (b) main deck cargo door (MDCD), with detail of the latch/hook positions.

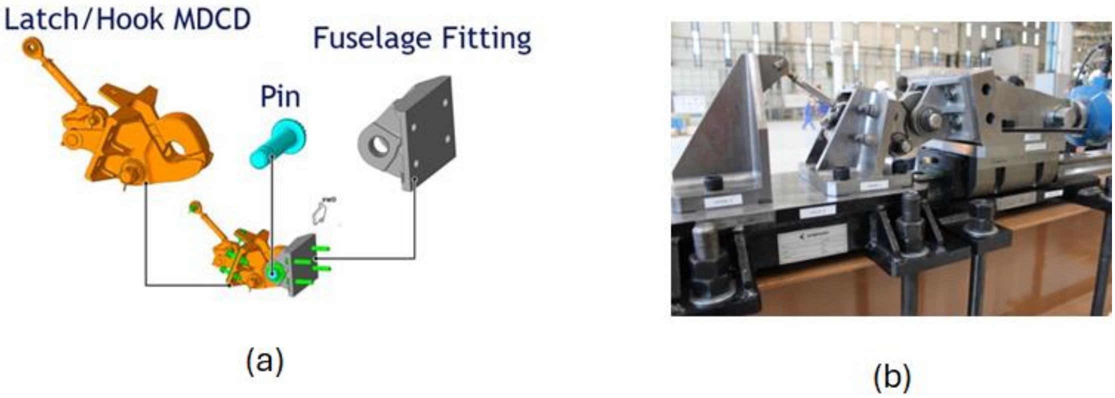

(a)

(b)

Figure 19 - Embraer E190F latch durability test overview. (a) latch configuration, (b) latch durability test setup and specimen.

4. COMPOSITE MATERIALS AND STRUCTURES

Composite Materials

A numerical and experimental study of fasteners as a delamination arrest mechanism in composite laminates under mode I loading (ITA - Ref. [8])

Summary:

This study presents a novel Semi-Analytical (SA) model to investigate Mode I delamination in Double-Cantilever Beam (DCB) composite specimens, incorporating the presence of holes and fasteners. The analysis aims to bridge the gap between experimental testing and computational modeling by offering a reduced-order analytical approach that accurately predicts delamination behavior while significantly reducing computational costs. The SA model is validated through a combination of experimental tests and Finite Element Analysis (FEA) using Cohesive Zone Modeling (CZM).

The research outlines the formulation of the SA model, which integrates the Rayleigh–Ritz method with an elastic foundation idealization to account for the presence of fasteners and their effect on crack arrest. The model's accuracy is demonstrated through comparisons with experimental data and FEA results, showing a strong correlation in terms of crack propagation, strain energy release rate, and overall failure behavior. Additionally, a parametric study highlights the influence of key parameters such as fastener placement, hole geometry, and material properties on delamination arrest effectiveness.

One of the main contributions of this work is the first known analytical method capable of including holes and fasteners in Mode I delamination analysis. The findings suggest that the SA model can serve as a viable alternative to traditional computationally expensive FEA simulations for preliminary damage assessment in composite structures. Furthermore, the study discusses the limitations of the analytical approach, particularly in capturing three-dimensional crack tip effects, and suggests future improvements, including extending the methodology to mixed-mode delamination and integrating it with higher-fidelity numerical techniques.

Highlights:

The experiment was conducted at the Laboratory of Aerospace Structures of the Aeronautics Institute of Technology (ITA) based on the ASTM D5528 standard. Twelve DCB specimens (Figure 20) were used in the experiment. All were manufactured via Hand Lay-Up (HLU) process using Hexcel® AS4/8552 unidirectional tape prepreg, made of carbon fiber-reinforced epoxy.

Four different configurations were tested in accordance with Table 1. For the C2 configuration, each specimen was reinforced with a stainless steel full thread socket head bolt and a stainless hex nut installed at the hole with a clearance fit. For C3 and C4 configurations, a standard aeronautical pin HST10BJ-6-2 made of 6AL-4V titanium alloy and a collar HST79CK-6 made of 7075 aluminum alloy were installed in the hole with a clearance fit.

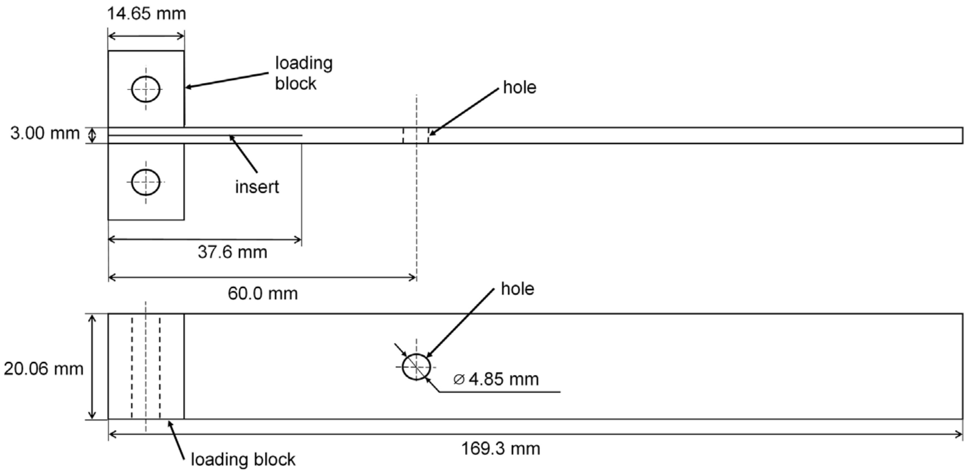

Figure 20 - Average dimensions of the DCB specimens.

Table 1 - Test matrix of the experiments

Code	Specimen	Type of fastener	Torque	# of Tests
C1	DCB with hole	none	–	3
C2	DCB with hole	conventional bolt and nut	finger tight ($\approx$ 0)	3
C3	DCB with hole	standard aeronautical fastener	1.69 N-m (15 in-lb)	3
C4	DCB with hole	standard aeronautical fastener	3.39 N-m (30 in-lb)	3

An Instron 5500R testing machine was used to apply displacement controlled loading on the specimens and measure the values of load and displacement. A constant opening displacement speed of 1 mm/min was applied by the machine and the load–displacement curves were recorded, as well as the crack lengths were noted down every millimeter when possible (Figure 21).

Figure 22(a) shows the specimen C4 at the end of the test. The arresting effect of the fasteners can be observed in Figure 22(b), where the average bending moment at the crack tip for each configuration is examined as a function of delamination length.

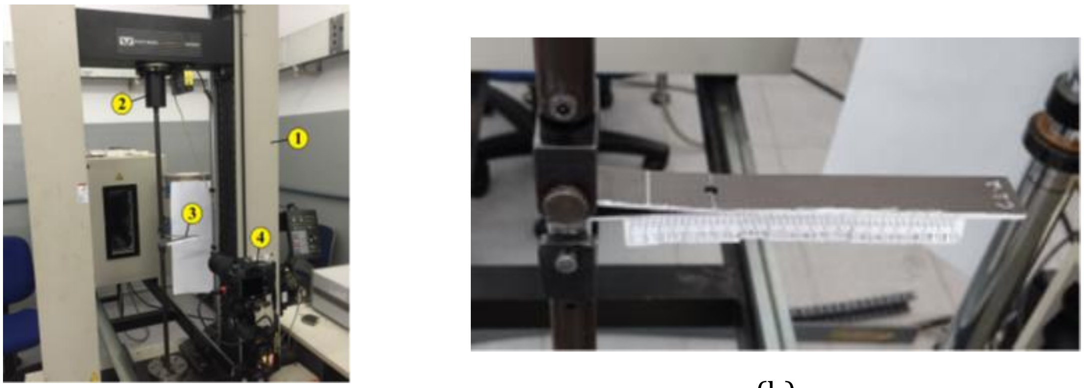

(a)

(b)

Figure 21 - (a) Experimental set-up: (1) Testing machine, (2) 2-kN load cell, (3) DCB specimen connected to the testing machine and (4) DSLR camera. (b) Crack propagation during experiment in a C1 specimen.

The value of strain energy release rate G_{IC} was calculated according to the ASTM standard by applying the Modified Beam Theory (MBT).

The SA model formulation is based on the Rayleigh–Ritz method to determine the displacement field of the DCB specimen. The mechanical and material properties are used in the Principle of Minimum Potential Energy (PMPE) to set up equilibrium equations. Once this system of equations is solved the displacement field is known. The displacement field will then be used in combination with the compliance method to determine the Strain Energy Release Rate (SERR), which in turn can be used to calculate the crack growth using a Newton–Raphson iteration method. The SA model is derived from the schematic shown in Figure 23. The symmetry of the DCB specimen is used to split it into halves, and it is placed on an elastic foundation.

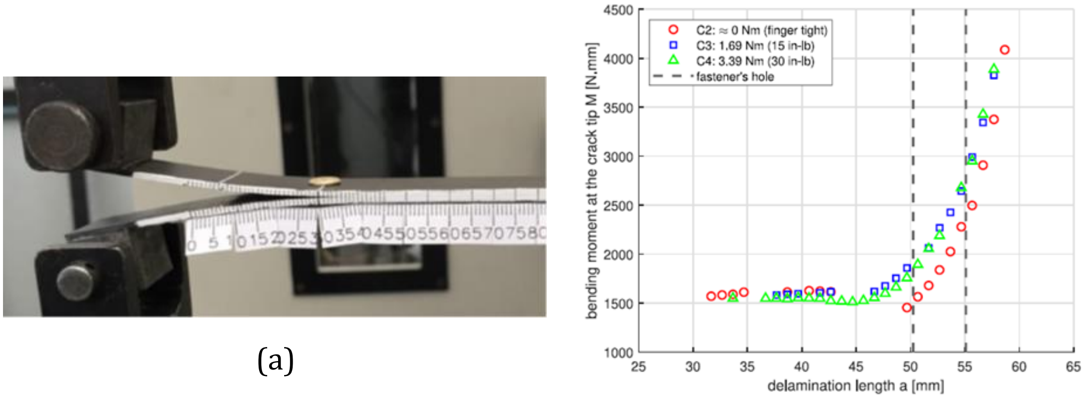

(a)

(b)

Figure 22 - (a) Specimen C4 at the end of the experiment with an opening load of 80N. (b) Comparison of required bending moment for crack propagation on specimens.

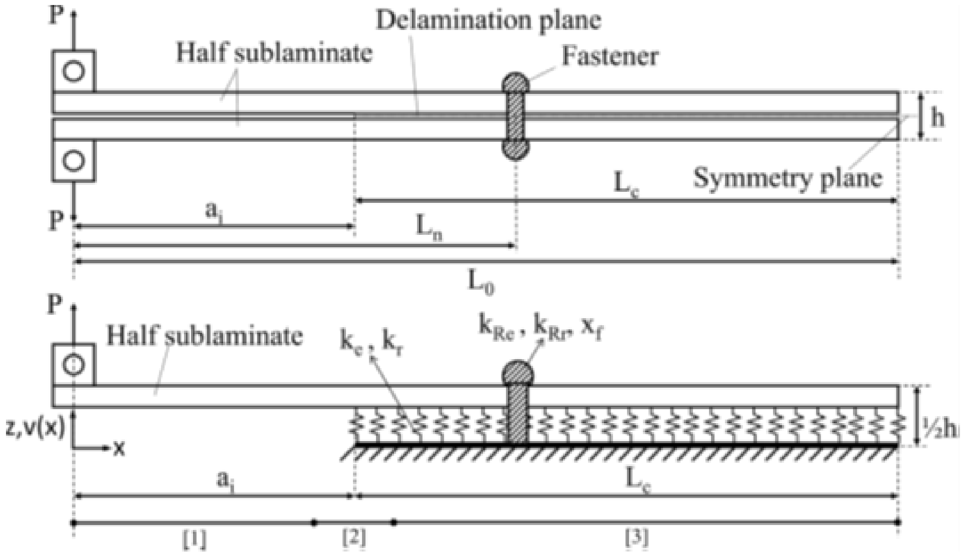

Figure 23 - Schematic of the DCB specimen for semi-analytical modelling.

The FE model used a fully 3D model (Figure 24) and the Cohesive Zone Model (CZM) was applied to represent the delamination propagation. In order to have a clear understanding of the effect of each feature, three models were analyzed: the first model created is a classical DCB specimen, then the same specimen is modelled containing a hole in lay-up stack direction and, finally, the fastened joint is added. These finite element models were all developed using the FE software ABAQUS®.

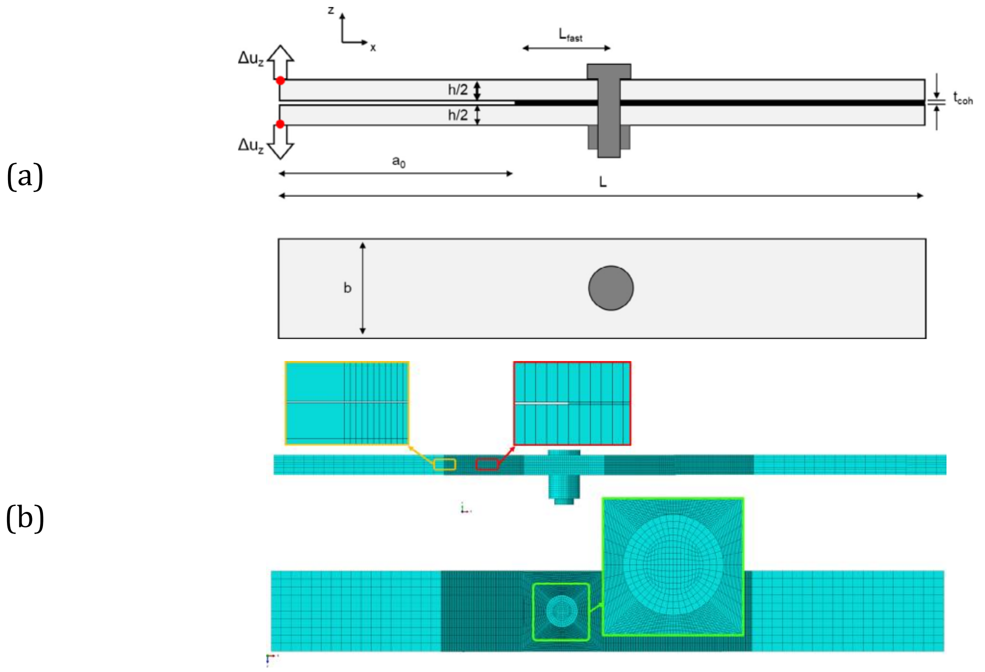

Figure 24 - (a) Finite element model schematic and (b) FEM mesh details.

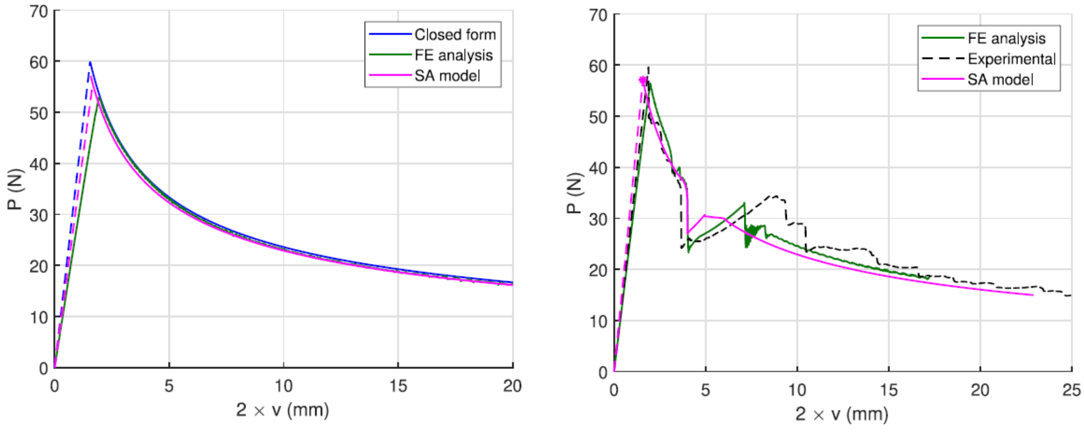

(a) (b)

Figure 25 - (a) Plot of the SA model of a plain DCB specimen against theory and (b) comparison of the SA model with a hole with FEA and experimental data.

In Figure 25(a), the main difference between the models is the linear opening behavior, where the FEA is more compliant than the closed loop and the SA model. The propagation behavior between the models is virtually identical, where the FEA splits the narrow difference between theory and the SA model. In Figure 25(b), the force opening behavior of DCB specimens with a hole is shown. After the crack propagation has been initiated, the response of crack propagation of the SA model and the experiment are matching until the crack reaches the hole in the specimen.

In Figure 26(a), the FEA shows that the crack tip keeps hanging on to the end of the hole. The first effect of this curvature is increasing the total length of the crack tip front by curving the crack tip from the hole to the sides, which in turn increases the forces necessary for the crack tip to grow. The secondary effect is that the curvature of the crack tip front also changes the loading mode of the crack tip.

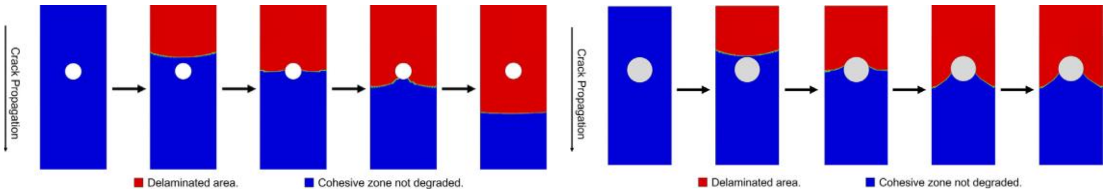

(a) (b)

Figure 26 - (a) Crack front progression in a DCB specimen with a hole and (b) Crack front progression in a DCB specimen with a fastener.

The opening stiffness after fastener initiation deviates from the stiffness found in the experiments. This could be a result of the earlier effects of the fastener. As the crack has not been allowed to grow as far as it would have been in the experiments, the opening arm in the SA model is shorter, which causes a stiffer opening behavior. Similar to the DCB specimen with the hole, the crack tip front is shaped as the hole and the fastener are initiated over the crack growth. This is shown by the FE analysis in both delamination and stress contours, Figure 26(b).

The results between the FE Model and Experimental results show an excellent correlation, confirming the high fidelity of the 3D numerical model developed to simulate the delamination propagation and the crack-arresting effect of the fastener under Mode I loading.

The effect of fiber orientation on fatigue crack propagation in CFRP: Finite fracture mechanics modelling for open-hole configuration (ITA - Ref. [9])

Summary:

The demand to capture translaminar crack growth under fatigue loading scenarios led this work contribution to carry out the Finite Fracture Mechanics (FFM) method in fatigue damage growth and the application of the Paris model to generate the translaminar damage propagation prediction. The purpose of this study is to analyze the effect of fiber orientation on translaminar crack propagation rate using the FFM model, which includes cycle damage increment estimation and fractographic analysis. The results confirm the feasibility of FFM in predicting crack growth and estimating life under cyclic loading. However, C-scan analysis and the revised crack propagation direction are critical in determining the realistic crack length, considering adhesive failure along the fiber direction. Additionally, this work contribution is also related to the application of the Paris model (based on dL/dN *vs* ΔK) to generate the translaminar damage propagation prediction model. The most dominant damage mechanism was the splitting pattern, which changed the aspect of failure for each laminate architecture as a function of fiber orientation. The laminate with multidirectional fiber orientation exhibited higher resistance to translaminar crack propagation due to the growth of splitting and delamination in multiple directions. The fiber orientation changed the propagation path, which influenced the fracture toughness and crack propagation rate behavior.

Highlights:

Laminated composites, particularly Carbon Fiber Reinforced Plastics (CFRP), have gained prominence in industrial applications due to their lightweight properties and sustainability advantages. However, the presence of open holes in structural components presents significant design challenges, as they act as stress concentrators, leading to crack initiation and propagation. Traditional fracture mechanics models, such as stress intensity factors and energy-based approaches, have limitations when applied to CFRP, necessitating the adoption of Finite Fracture Mechanics (FFM).

The FFM model is based on energetic principles, where the energy required for crack propagation is related to material fracture toughness. The model incorporates stress intensity factors and laminate-specific parameters to predict crack length. Experimental validation involved tensile testing of open-hole laminates under cyclic loading, revealing that damage progression depends on fiber orientation. Left side of Figure 27 illustrates the translaminar crack failure modes, highlighting the stress distribution near the hole edges. The analysis also considers correction factors for stress intensity and finite width effects. Furthermore, the right side of Figure 27 provides a methodological flowchart detailing the computational steps for predicting crack length and damage evolution.

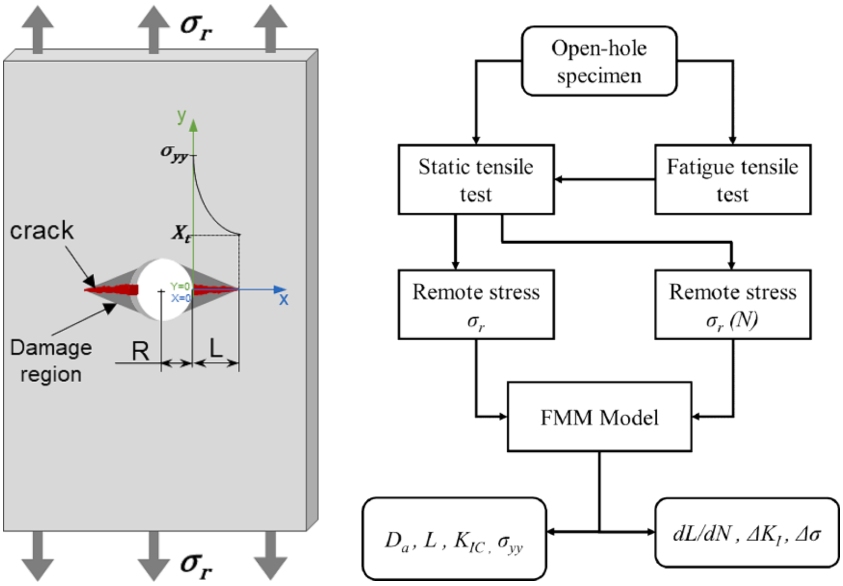

Figure 27 - On the left, translaminar cracks failure mode under an opening mode loading. On the right, methodology flow chart.

The CFRP laminates were fabricated using a resin transfer molding (RTM) process, with two fiber orientations: cross-ply $[0/90]_{4S}$ and quasi-isotropic $[\pm45/0/90]_{2S}$. The mechanical properties were determined according to ASTM standards, and fatigue testing was conducted under controlled cyclic loading conditions. *Figure 28* shows ultrasonic C-scan images capturing damage evolution over cycles. The experimental results indicate that quasi-isotropic laminates exhibit more damage resistance due to multidirectional fiber distribution, whereas cross-ply laminates show localized crack propagation along the fiber direction.

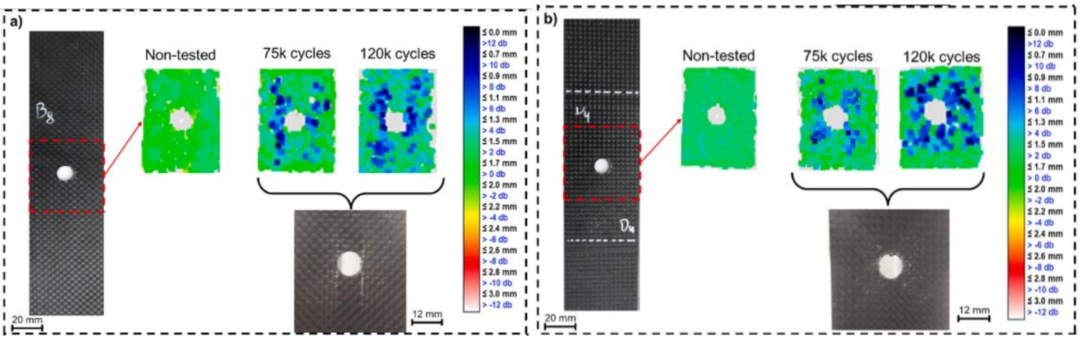

Figure 28 - C-scan considering cyclic loading: a) [0/90] and b) [±45/0/90].

The mechanical test results demonstrate a significant reduction in residual strength due to cyclic loading, with the cross-ply laminate experiencing a 36% reduction in strength compared to 20% for the quasi-isotropic laminate. Damage length increases with cycles, affecting residual stress and stress intensity factor (SIF). The quasi-isotropic laminate exhibits slower crack growth due to enhanced splitting and delamination resistance, as confirmed by C-scan imaging in Figure 28. Figure 29(a) presents a scheme of crack length development as a function of cycles. The study introduces a revised crack length formula to account for crack orientation effects, correcting for fiber-angle-induced deviations. Figure 29(b) illustrates the impact of fiber orientation on crack direction, where quasi-isotropic laminates display 45° crack propagation compared to the perpendicular propagation in cross-ply laminates.

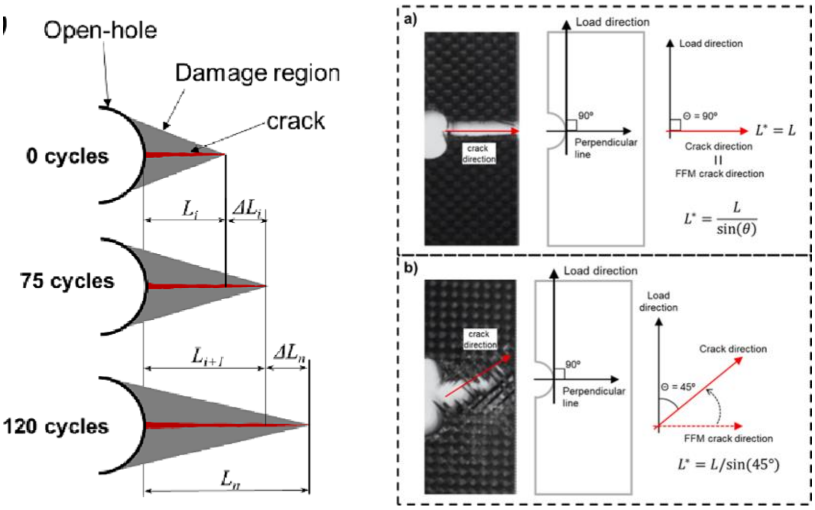

Figure 29 - On the left, crack length development as a function of cycles. On the right, crack orientation: a) [0/90] and b) [±45/0/90].

The Paris model is applied to predict damage progression rates under fatigue loading. Quasi-isotropic laminates require more energy for crack growth due to mixed-mode fracture behavior. Fractographic analysis identifies key failure mechanisms: cross-ply laminates exhibit broom-like fracture patterns with translaminar propagation, whereas quasi-isotropic laminates develop a sawtooth fracture pattern due to fiber interaction effects. The fracture surface analysis in Figure 30 highlights interlaminar delamination in quasi-isotropic laminates, further validating their superior fatigue resistance.

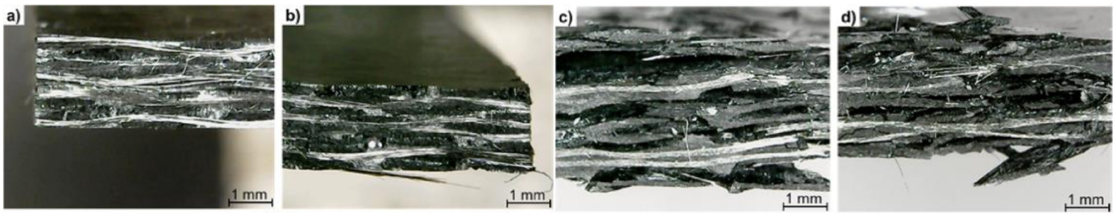

Figure 30 - Fractured surface (thickness section): (a-b) [0/90] and (c-d) [±45/0/90].

This study confirms that fiber orientation significantly influences fatigue damage progression in CFRP laminates. The quasi-isotropic lay-up demonstrates superior crack growth resistance due to multidirectional splitting and delamination, whereas the cross-ply lay-up exhibits faster crack propagation along fiber-aligned paths. The integration of FFM and the Paris model provides accurate predictions of damage growth, with experimental validation through ultrasonic C-scan imaging. The revised crack propagation model, incorporating fiber orientation effects, offers a more realistic assessment of fatigue life in open-hole CFRP laminates.

Investigation on Induced Intra/Interlaminar Damage Propagation in CFRP Subjected to Cyclic Tensile Loading After Impact (ITA - Ref. [10])

Summary:

Impact damage to composite structures results in multiple, complex failure modes, often requiring the replacement of entire components and thereby escalating aircraft maintenance costs. To address that issue, the present study investigates the damage propagation behavior with particular emphasis on intra- and interlaminar failure modes. Carbon fiber/epoxy composites were subjected to tensile after impact (TAI) fatigue tests at different energy levels to induce different damage modes and extents within the specimens. A non-destructive testing technique (C-scan) was used to assess the interlaminar damage propagation, while the intralaminar fracture toughness of the post-impact specimens was characterized using a finite fracture mechanics model. The results show that the crack propagation behavior is strongly influenced by the initial impact damage characteristics, in particular the impact energy level. Lower impact energies tend to promote interlaminar failure modes leading to fatigue crack propagation by delamination. Conversely, higher impact energy levels induce fiber fracture, resulting in a self-similar relationship between intra- and interlaminar propagation.

Highlights:

Carbon fiber/epoxy composite laminate specimens were manufactured by resin transfer molding (RTM) in a quasi-isotropic lay-up configuration. The mechanical tests performed include low-velocity impact (LVI) for low and high energy, tensile tests with the impact damage at the central region of the specimen and fatigue tests. C-scan images were obtained through acoustic ultrasound inspection. Figure 31 illustrates the test steps and data analysis carried out. The collected data was analyzed using the finite fracture mechanics (FFM) model combined with interlaminar growth analyses using C-scan techniques.

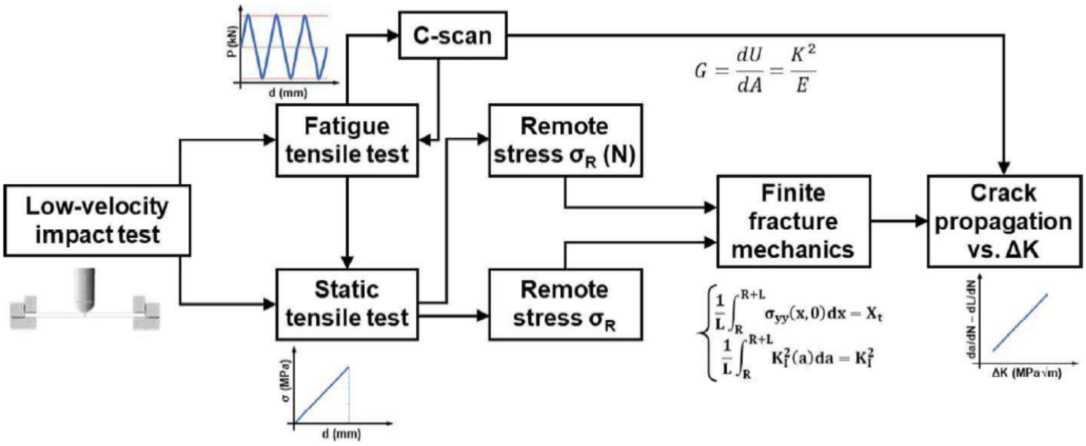

Figure 31 - Work flowchart following test procedure and data analysis.

For the drop test, low energy (LE) level exhibited lower energy dissipation due to internal delamination fractures and limited intralaminar fractures. High Energy (HE) levels presented a greater extent of material fracture.

Post-impact cyclic stress loading was applied to the impacted laminates. Figure 32 shows the C-scan of non-impacted laminate and the impact curve, besides the backside of the impacted laminate and ultrasound results after cyclic loading. Low-energy laminates primarily exhibited delamination, and high-energy laminates exhibited increased fiber fracture.

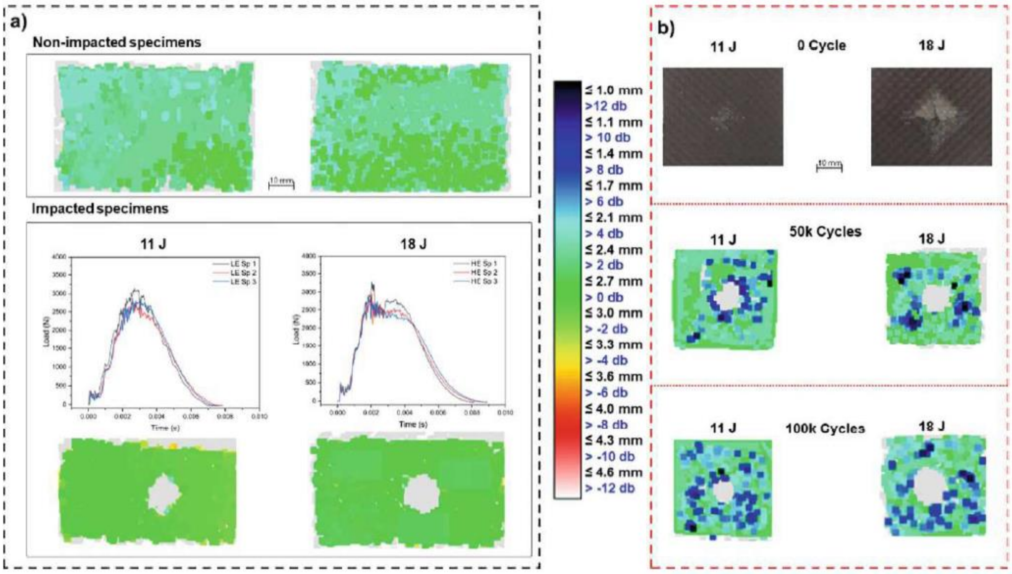

Figure 32 - Mechanical test analysis: (a) impact test curve and C-scan images, and (b) propagation of interlaminar fatigue damage (C-scan images).

For cyclic loading of impacted samples, the crack initiates in the matrix and propagates along the fiber-matrix interface following the fiber direction, promoting interlaminar propagation. Static tests promote intralaminar fractures perpendicular to the fiber direction, rupturing the fiber. The static tensile test was then used to evaluate residual stress. HE presents lower damage propagation through delamination due to translaminar damage.

Figure 33 shows the residual stress, the growth rate of interlaminar and intralaminar damages as a function of cycles for each post-impact energy level and the curves based on the power law curve.

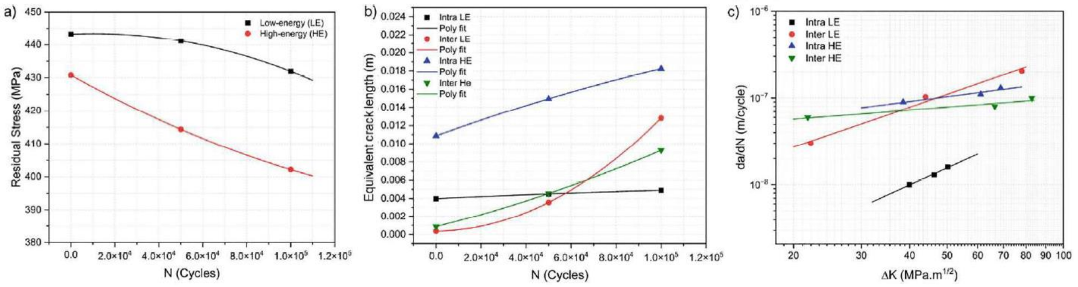

Figure 33 - (a) SN curve, (b) compliance curve: equivalent crack length vs. cycles, and (c) Paris curve: crack propagation rate versus stress intensity factor.

The results show that the crack propagation behavior is directly influenced by the amount and type of initial damage. Low energy impacts lead to a more rapid absolute increase in interlaminar cracking. Increased impact damages shift the initial failure modes, indicating a synergistic interaction between intra and interlaminar failure mechanisms.

Data reduction methods in the fatigue analysis of the Double Cantilever Beam, Part I: Fundaments and Virtual fatigue testing (USP - Ref. [11])

Data reduction methods in the fatigue analysis of the Double Cantilever Beam, Part II: Evaluation and case studies (USP - Ref. [12])

Summary:

The characterization of high-cycle crack growth properties of bonded joints is an important research field with a direct impact on the practical engineering and designing of composite structures. Regardless, to date, no standard exists to evaluate the Mode-I fatigue properties of adhesively bonded joints, and thus several different reduction approaches have been used by researchers. In part I of this work, we explore these approaches and show what differences emerge when trying to obtain the rate of crack propagation curves traditionally used in fatigue analysis. A difference of more than 2.5 times in the rate of crack propagation was observed depending on the method used in the analysis. It is further shown that the discrepancies in the results decrease drastically when the equivalent crack concept is employed, rather than relying on visual crack measurements. Finally, it is proposed that virtual fatigue tests can be used to investigate the accuracy of the different reduction methods.

To date, no standard exists to evaluate the Mode-I fatigue properties of adhesively bonded joints nor for delamination of composite structures. In part II of this work, virtual fatigue tests are used to explore several reduction schemes that have been employed by researchers to characterize the Paris law coefficients. The results show that different reduction methods can yield different Paris curves when the measurement of the actual crack size is used, and the discrepancy among the methods increases as the global stiffness of the joint increases. However, when the concept of equivalent crack is used, the performance of most reduction methods increases significantly. The results show that the use of the equivalent crack concept combined with an appropriate reduction method can yield very accurate results, sparing cumbersome crack length measurements altogether.

Highlights:

The crack growth rate is correlated with the maximum strain energy release rate (G_{max}) using Paris' law. Accurately determining G_{max} is crucial and depends on the method used to estimate crack length. Several reduction schemes are employed, including Simple Beam Theory (SBT), Timoshenko Beam Theory (TBT), Compliance-Based Beam Model (CBBM), Beam on Elastic Foundation Models (BEFM), and Penado’s method, as well as Corrected Beam Theory (CBT) and Compliance Calibration Method (CCM).

Virtual fatigue tests using finite element modeling (FEM) were developed and validated with experimental data, demonstrating their ability to replicate real fatigue behavior. Static damage was based on a Cohesive Zone Model (CZM) and triangular traction-separation law. Fatigue damage was based on a model with two parts: an initialization step and an actual fatigue step, as represented in *Figure 34*.

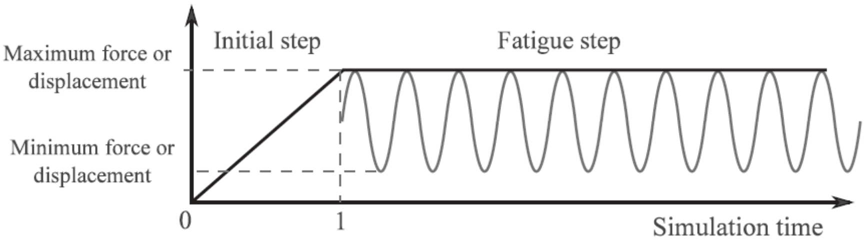

Figure 34 - Strategy used for modeling fatigue cycles.

Figure 35 shows the fitted curve and visual crack measurements of experimental data, as well as the SERR versus the number of cycles for each reduction method and its obtained Paris curve. The differences in the rate of crack propagation can be more than twice depending on the reduction method employed in the analyses.

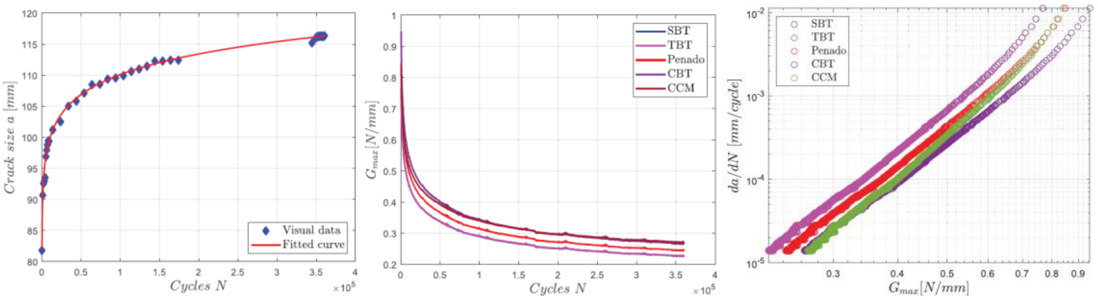

Figure 35 - On the left, visual crack size measurements and fitted curve; in the middle, maximum SERR versus number of cycles for each reduction method; on the right, crack growth curves obtained from each reduction method. All using visual crack measurements.

Figure 36 shows crack size values obtained by each reduction method and compares them with the experimental results measured visually, using equivalent crack size (including CBBM and excluding CBT and CCM methods), as well as values of the SERR obtained when using the equivalent crack size of each method and the Paris' curves.

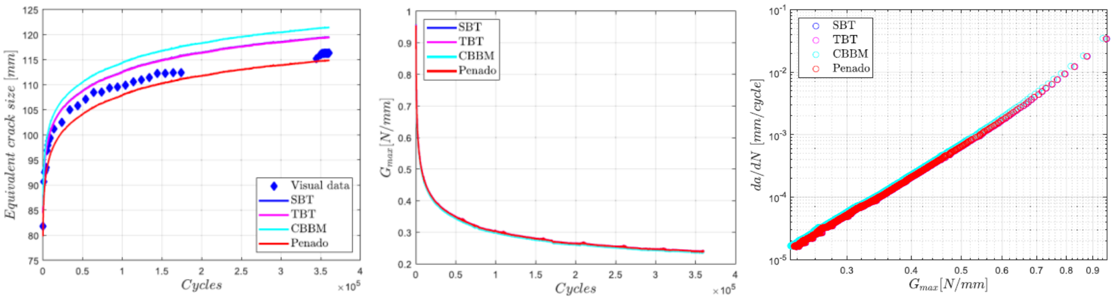

Figure 36 - On the left, equivalent crack size for each reduction method; in the middle, maximum SERR versus number of cycles for each reduction method; on the right, crack growth curves obtained from each reduction method.

In order to determine the best reduction method, FEM virtual fatigue tests were performed using Paris coefficients as inputs. These tests were validated by comparison of numerical results against numerical data. Results showed a good correlation between the experimental and virtual tests, and the model was able to replicate the compliance values. Figure 37 shows a comparison between delamination growth rate calculated from the virtual test with the analytical one imposed in the numerical model for both metallic and composite specimens.

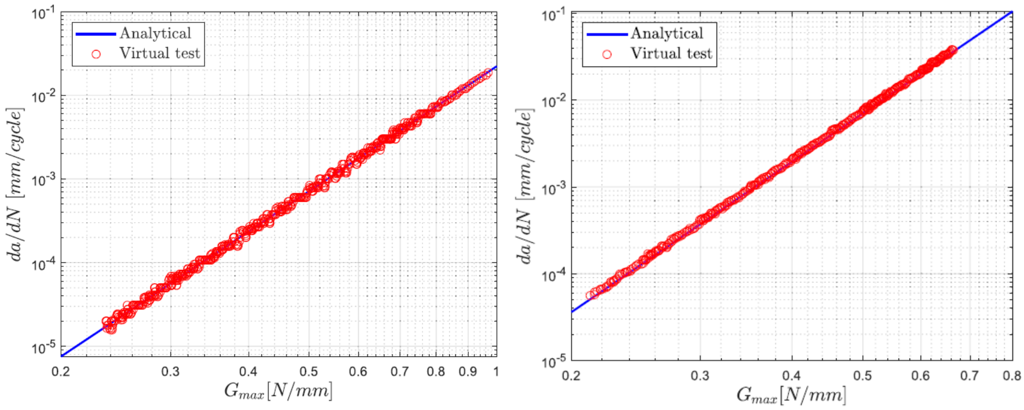

Figure 37 - Comparison between the analytical crack growth rate imposed in the model and the actual crack growth rate calculated from the virtual test for crack growth in metallic DCB (left) and composite specimen (right).

The numerical model was validated for the case of crack propagation in a bonded DCB with metallic adherents and for the case of delamination growth in a composite DCB. The virtual fatigue tests considered were shown to produce results equivalent to that of real fatigue tests.

In order to evaluate the performance of the data reduction schemes, four different setups of virtual high cycle fatigue tests are investigated in Part II: DCB made of thin aluminum under displacement control, DCB made of thick aluminum under displacement control, DCB made of thick steel under force control, and delamination in composite DCB under displacement control. Figure 38 shows the comparison between the equivalent crack obtained from the reduction methods and the crack size measured directly from the virtual tests (FEM) for the aluminum specimens.

The same analysis was made for measured crack, adding CBT and CCM methods and excluding CBBM method, as shown in Figure 39 for aluminum.

The equivalent crack length estimates varied significantly among methods, with equivalent crack approaches yielding more consistent Paris curves. The use of measured crack length methods led to greater discrepancies, especially in high-stiffness specimens.

For the thin aluminum DCB, reduction methods based on the equivalent crack concept produced reliable results, with CBBM providing the best estimation of crack growth rates. In the thick aluminum DCB, the Penado method showed the highest accuracy, while SBT and TBT methods overestimated crack growth by more than 50%.

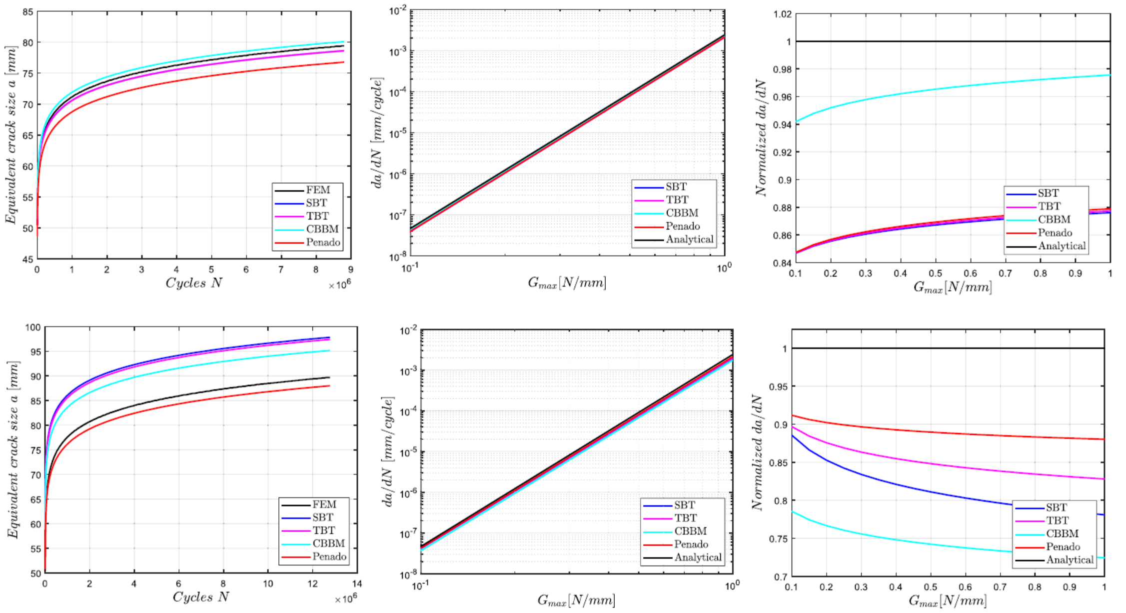

Figure 38 - On top, thin aluminum DCB equivalent crack size for different compliance theories (left), fatigue crack growth rate (middle) and normalized growth rate (right) versus maximum SERR; Under, thick aluminum DCB equivalent crack size for different compliance theories (left), fatigue crack growth rate (middle) and normalized growth rate (right) versus maximum SERR.

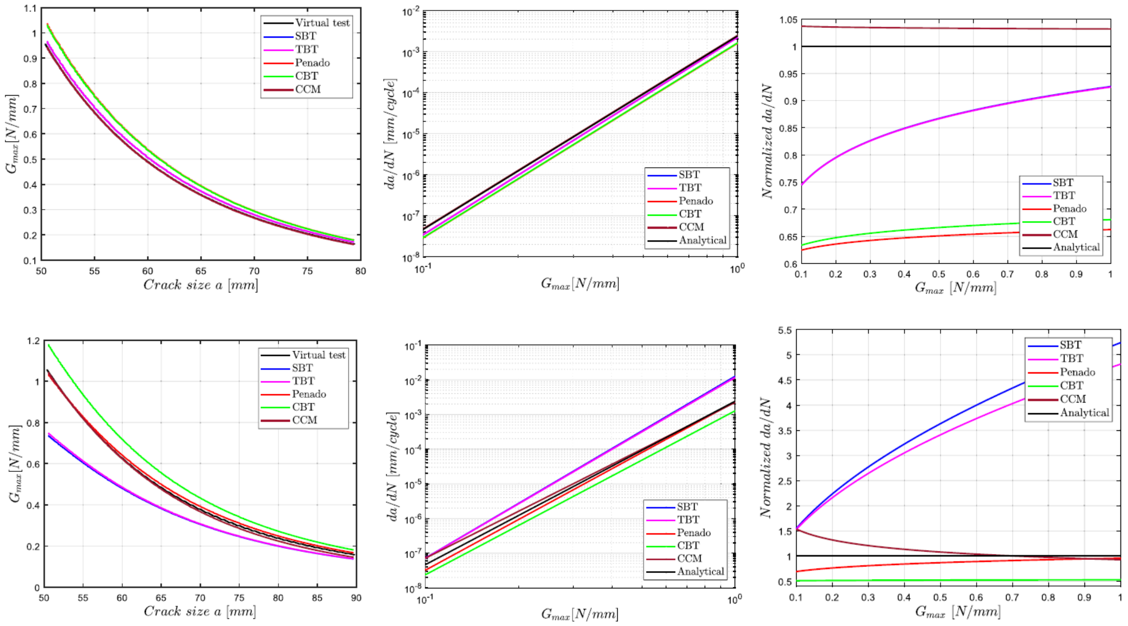

Figure 39 - On top, thin aluminum DCB maximum SERR evolution for different compliance theories with measured crack length (left), fatigue crack growth rate (middle) and normalized growth rate (right) versus maximum SERR; Under, thick aluminum DCB maximum SERR evolution for different compliance theories with measured crack length (left), fatigue crack growth rate (middle) and normalized growth rate (right) versus maximum SERR.

The thick steel DCB was tested under force control to analyze the effects of increasing strain energy release rate (G_{max}) during fatigue testing. Equivalent crack methods remained consistent, with Penado's approach showing the best fit to the imposed Paris curve. Measured crack length methods, on the other hand, performed poorly, with SBT and TBT overestimating crack growth by up to ten times. CBT and Penado's method yielded the most accurate results for measured crack length analyses.

A virtual fatigue test was performed on a Carbon Fiber Reinforced Plastic (CFRP) DCB specimen to evaluate the reduction methods for composite materials. CBBM produced the most accurate results when using the equivalent crack concept, whereas SBT, TBT, and Penado's method tended to overestimate crack growth. Measured crack length methods showed significant variations, with CBT and CCM performing better than SBT and TBT.

The findings confirm that equivalent crack methods improve the accuracy of fatigue crack growth characterization and should be preferred over direct crack measurement approaches. The study demonstrates that Penado's method performs best for high-stiffness metallic specimens, while CBBM is most reliable for composite specimens. Measured crack length methods introduce significant errors, particularly in thick DCB specimens.

Progressive intralaminar damage in woven composite materials under mixed-mode fracture (ITA - Ref. [14])

Summary:

The civil aviation industry has adopted strict requirements in the design of structural components, aiming to achieve lower emission levels with economically viable aircraft from the point of view of manufacturing and operation. For this task, composite materials have been commonly adopted as potential materials allowing the design of damage tolerant tailored structures with high stiffness and strength with low weight. Therefore, a deep understanding of fracture and fatigue in composites is a topic of interest for the modern aviation industry. Damage in composites is often classified as intralaminar and interlaminar. Interlaminar damage occurs at the matrix interface between layers, and benefits from a robust methodology for damage tolerance evaluation using both analytical and numerical approaches. However, for the intralaminar case, different failure mechanisms are associated resulting in analytical and numerical frameworks that are not yet completely explored. Furthermore, the introduction of mixed-mode loading on intralaminar damage requires a combination of different failure characteristics which are dependent on the reinforcement material architecture. This thesis explores the quasi-static mixed-mode loading fracture of woven composite materials and aims to provide a methodology for damage tolerance analysis, regarding the intralaminar damage. A Modified Arcan Fixture is proposed for fracture characterization (Figure 40), as a standard testing practice for mixed-mode is non-existent. Through strain monitoring using the digital image correlation technique, an analytical fracture initiation criterion was proposed for mixed-mode fracture. A finite element numerical model was implemented, with the objective of using material properties only as input data. For the modelling strategy implemented, the model displays a good correlation to the observed failure mechanisms, with an over prediction of the maximum load capacity under some mixed-mode conditions. The finite element model formulation was extended to handle cyclic load cases assuming a Paris Law for crack propagation rate, in accordance with experimental data on the scientific literature.

Highlights:

To characterize mixed-mode fracture, the study developed a non-standard testing device based on the Modified Arcan Fixture (MAF). Specimens were manufactured using a woven composite laminate and subjected to controlled loading conditions. The Digital Image Correlation (DIC) technique was employed for strain monitoring, enabling accurate fracture analysis. Figure 41 illustrates the strain monitoring setup using DIC, highlighting its capability to capture detailed deformation fields. The study also introduced a novel toughness calculation method based on R-curves extracted from experimental data.

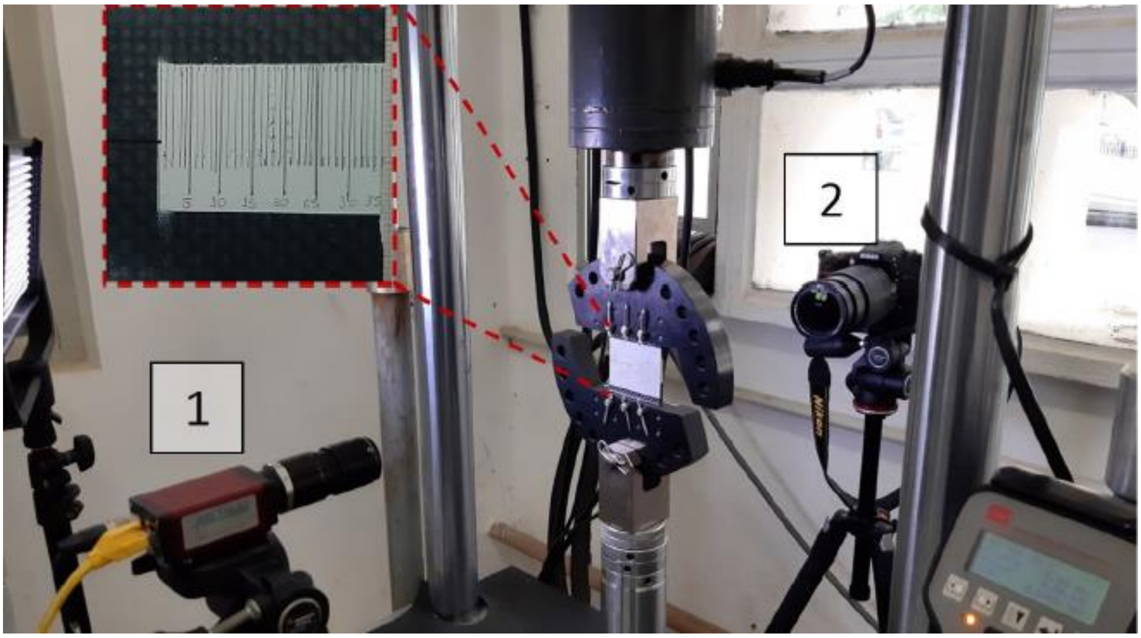

Figure 40 - Experimental setup, with Arcan Fixture.

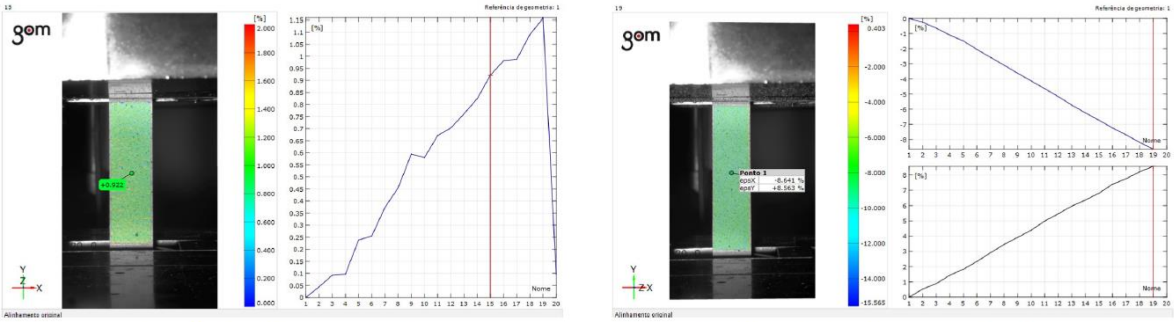

(a) Tensile loading on $(0)_8$ layup

(b) Tensile loading on $(45)_8$ layup

Figure 41 - Strain monitoring using Digital Image Correlation.

The experimental results revealed distinct failure modes under different loading conditions. Mode I loading led to crack opening with fiber bridging, whereas Mode II loading resulted in shear-driven delamination. Mixed-mode loading exhibited a combination of these behaviors, with crack propagation influenced by fiber orientation and stress distribution. Figure 42 presents load versus displacement plots for an example of specimen configuration, demonstrating the influence of mixed-mode effects on mechanical response. Furthermore, numerical modeling using the Finite Element Method (FEM) showed good correlation with experimental results, although an overestimation of maximum load capacity was observed under some conditions. The finite element model was further extended to include fatigue damage, implementing a Paris Law-based crack propagation framework. Figure 43 illustrates the crack propagation rate evolution, showcasing the model's ability to predict fatigue behavior.

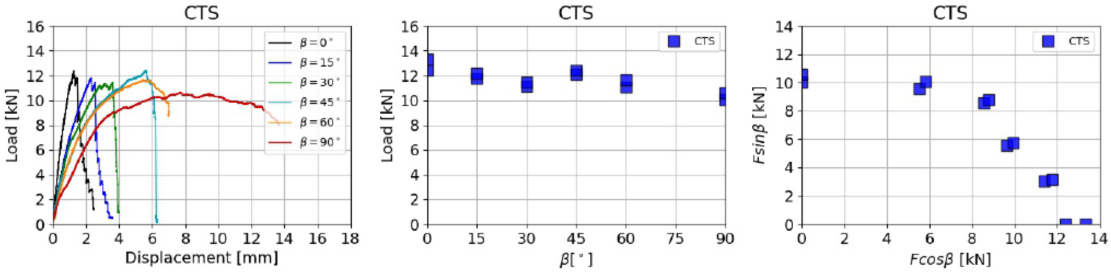

Figure 42 Load vs displacement plots for CTS specimens.

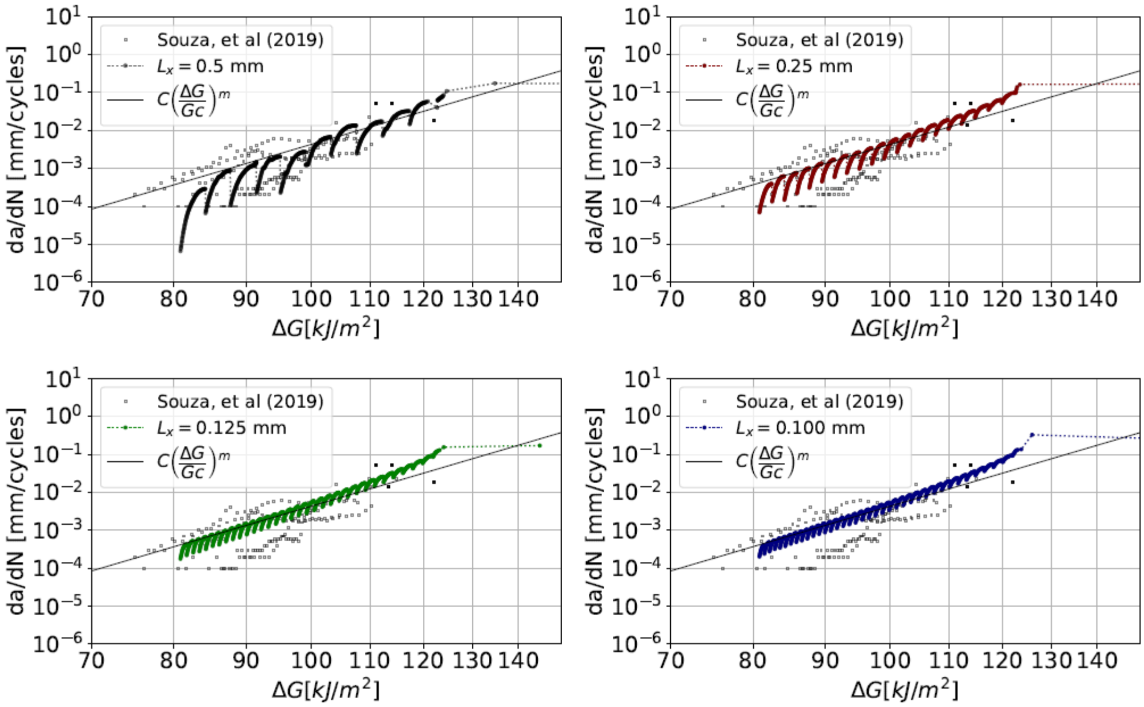

Figure 43 - Crack propagation rate evolution.

The novel methodologies proposed, including the MAF-based testing procedure and DIC-driven toughness calculations, offer valuable tools for future research. While the numerical model demonstrated high accuracy in capturing failure mechanisms, further refinement is needed to enhance its predictive capabilities under complex loading scenarios. Future work should focus on refining fatigue modeling approaches and validating findings across different composite material systems.

Manufacturing Deviations in Composite Fastened Joints (Embraer)

Summary:

Embraer conducted a technology development project related to mechanical tests at coupon level addressing the effect of manufacturing and assembly deviations on the strength of composite fastened joints.

Several types of manufacturing and assembly deviations were assessed, such as reduced fastener edge, reduced fastener pitch, hole with bad quality, and excessive washer and shim usage.

The test campaign evaluated the strength of carbon fiber reinforced plastic coupons through tensile bearing tests under static and fatigue loading, at different environmental conditions. Test specimens were assessed in pristine (intact) condition and with manufacturing deviations intentionally included.

The data obtained allowed a better assessment of the criticality of each defect type by engineering teams when giving disposition on non-conformities in the manufacturing of composite components.

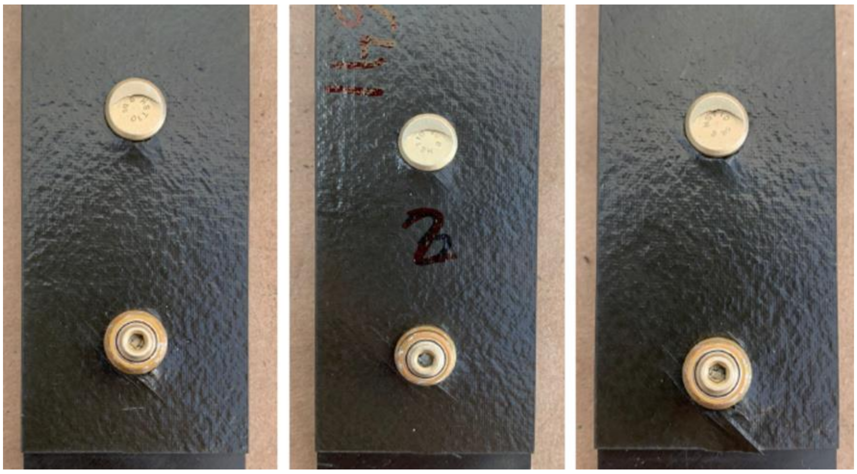

Figure 44 - Typical failure modes at composite fastener joints with manufacturing deviations.

Composite Structures

EVE-100 development (Embraer)

Summary:

Eve Air Mobility, an independent company founded by Embraer, is at the forefront of developing the EVE-100, an electric vertical takeoff and landing (eVTOL) aircraft designed to revolutionize urban air mobility. The EVE-100 is engineered to accommodate four passengers and one pilot, aiming to provide efficient and sustainable urban transportation solutions.

In July 2024, Eve revealed its first full-scale eVTOL prototype (Figure 45), marking a significant step in the aircraft's development. By January 2025, the EVE-100 prototype underwent ground testing, including the initial firing of its pusher engine, a crucial component for forward flight.

The Brazilian National Civil Aviation Agency (ANAC) released Eve's proposed airworthiness criteria for public consultation in December 2023, advancing the certification process. Within this proposal, EVE.2240 requirement supplies the present proposals for compliance with structural durability for this class of aircraft.

Figure 45 - EVE-100 first prototype (picture by Embraer).

5. HYBRID STRUCTURES

Processing understanding, mechanical durability and hygrothermal stability of PC/AA6061 hybrid joints produced via injection overmolding (UFSCar/ TU-Graz - Ref. [15])

Summary:

In the present study, single-lap joints of Polycarbonate (PC) and laser-textured aluminum alloy AA6061 were manufactured by Injection Overmolding (IOM) and characterized in terms of microstructure, quasi-static and long-term mechanical performance and hygrothermal stability. The injection overmolding parameters were optimized through design of experiments and analysis of variance, which showed that the parameters of barrel temperature, injection speed and holding pressure positively affected the Ultimate Lap-Shear Force (ULSF). PC/ AA6061 injection overmolded hybrid joints exhibited outstanding joining strength of 7.2 ± 0.5 MPa. Under fatigue cyclic loading, hybrid joints produced with optimized IOM processing conditions showed a fatigue life of 35% ULSF at 10^6 cycles, demonstrating excellent mechanical durability. Moreover, PC/AA6061 injection overmolded hybrid joints showed good hygrothermal stability, with no significant variations in joining strength after aging in water at 80°C for 30 days.

Highlights:

PC/AA6061 single-lap joints were fabricated by IOM, where laser-textured AA6061 surfaces were overmolded with commercial grade PC. The dimensions of the joint and overlap region were adapted from the ASTM D1002 standard. Key parameters such as barrel temperature, injection speed, and holding pressure were optimized using a Design of Experiments (DoE) approach, while holding time, mold temperature and cooling time were kept constant. Figure 46 shows the specimen. Mechanical testing included lap-shear (ASTM 1002) and fatigue testing, while hygrothermal stability was examined through water immersion at 80°C for up to 30 days (ASTM D1151). Fracture surfaces were analyzed using Confocal Laser Scanning Microscopy (CLSM) and Scanning Electron Microscopy (SEM).

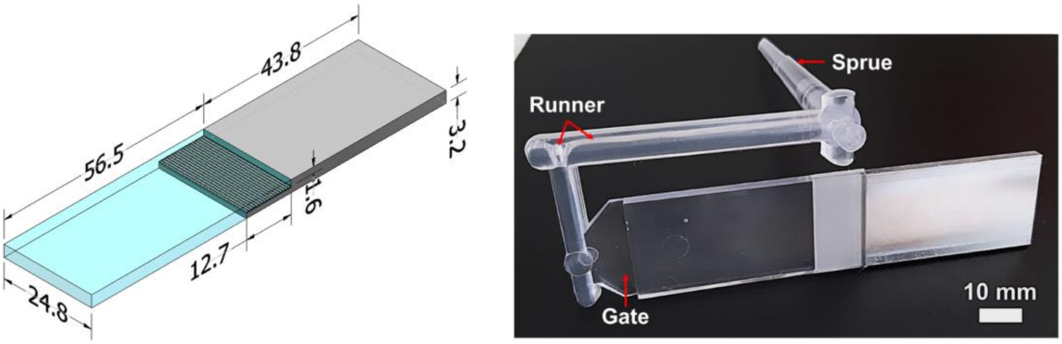

(a) (b)

Figure 46 - (a) Geometry and dimensions (in mm) of the injection overmolded PC/ AA6061 hybrid joint specimen. AA6061 in light gray, (b), photograph of an injection overmolded PC/AA6061 joint specimen containing the sprue, runner and gate.

The ultimate lap-shear force (ULSF) was positively influenced by barrel temperature, holding pressure, and injection speed. Optimized conditions (330°C barrel temperature, 80 cm^3/s injection speed, 1000 bar holding pressure) resulted in an average ULSF of 2149 N (~7.2 MPa shear strength). Figure 47 shows polymer fracture surfaces and cross-sections of PC/AA6061 joints.

6.

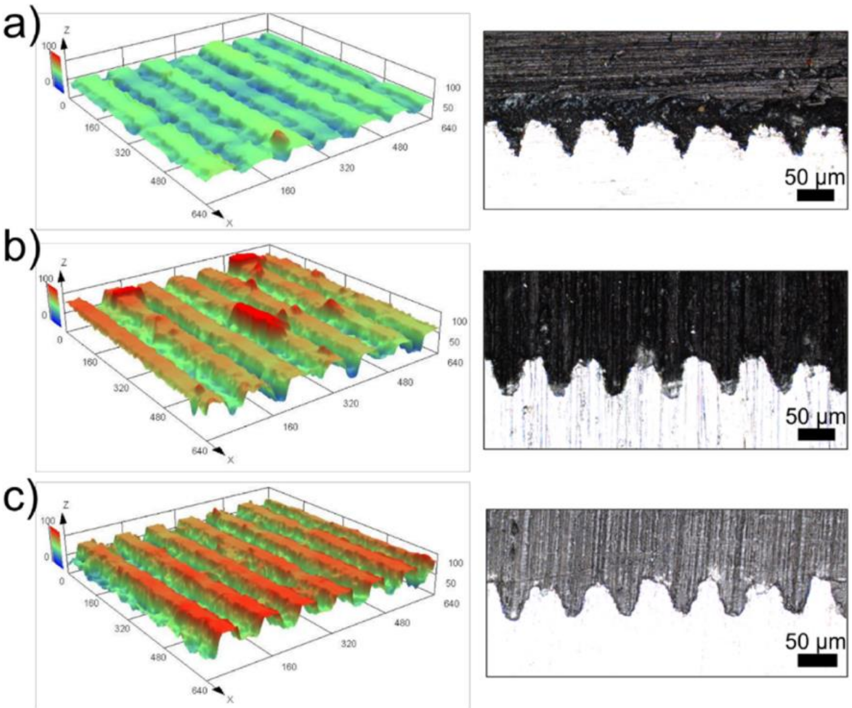

Figure 47 - On the left, laser confocal microscopy images of polymer fracture surfaces and the right-hand side images obtained in the laser confocal microscope of the cross-section of PC/AA6061 joints injection overmolded under the following conditions: a) C1 (minimum levels); b) (center point – CP); and c) (maximum levels). In the cross-section images, metal and polymer parts appear as light and dark, respectively.

Fatigue testing results, depicted in Figure 48, revealed outstanding mechanical durability, with joints enduring up to 10^6 cycles at 30% ULSF. The failure mechanisms, illustrated in Figure 48, were influenced by the degree of polymer penetration into laser-textured grooves.

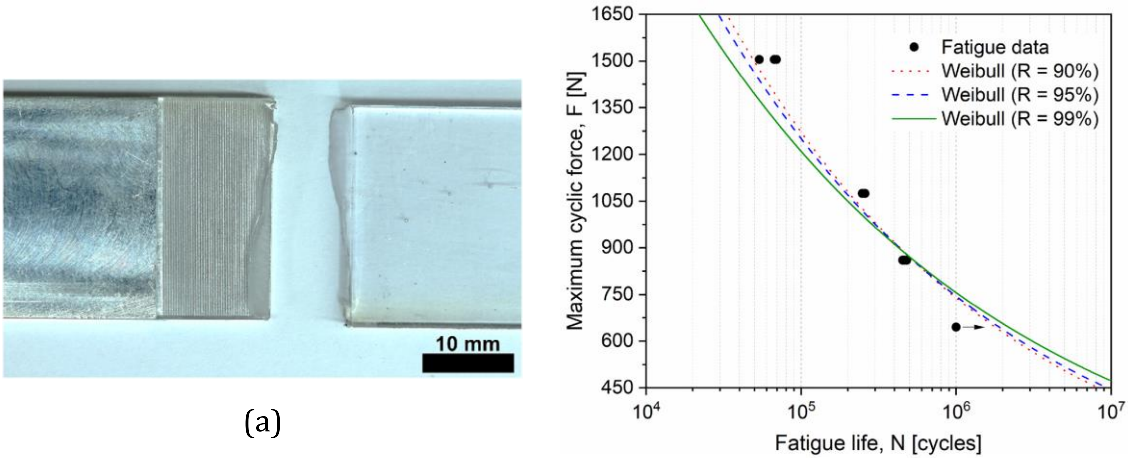

(a)

(b)

Figure 48 - (a) photograph exemplifying the failure mode of the PC/AA6061 joints injection overmolded in the optimized condition subjected to fatigue, (b) force-life (F-N) curve in tensile mode (R=0.1).

The study demonstrates that IOM can produce high-strength, durable PC/AA6061 hybrid joints. The combination of optimized processing parameters and laser surface texturing enables excellent adhesion, fatigue resistance, and hygrothermal stability, making these joints viable for aerospace applications.

6. STRUCTURAL HEALTH MONITORING

On the Strain-Sensing Capabilities of a Novel All-Solid-State Sodium-Based-Electrolyte Battery Under Vibration Loads (U.Porto/USP - Ref. [16])

Response of a Novel All-solid-state Sodium-based-electrolyte Battery to Quasi-static and Dynamic Stimuli (U.Porto/USP - Ref. [17])

Summary

The growing environmental concerns and the need for sustainable energy solutions have driven research toward alternatives to Lithium-Ion Batteries (LIBs). Solid-state Sodium-Based Batteries (SSBs) have emerged as a promising solution due to their cost-effectiveness, high performance, and environmental benefits. In addition to energy storage, recent studies suggest these batteries might also serve as strain sensors, enhancing their multifunctionality. This study investigates the potential of an all-solid-state sodium-ion-based ferroelectric battery as a strain-sensing device under vibrational loads. The goal is to explore its viability for use in self-powered Structural Health Monitoring (SHM) systems.

Lithium-ion batteries dominate the energy storage market, but they have several limitations, including high costs, reliance on scarce materials, and safety concerns due to flammability. Sodium-ion batteries present a viable alternative due to their abundance, cost-effectiveness, and stability. Additionally, advancements in solid-state electrolytes have opened new possibilities for sodium-ion batteries, enhancing their mechanical properties and enabling novel applications such as structural sensing.

SHM is an essential practice in aerospace, civil engineering, and automotive industries, aimed at detecting and preventing structural failures. Traditional SHM systems rely on external sensors, which require power sources and additional wiring. A self-powered sensing battery that can both store energy and detect strain could revolutionize this field, providing a more integrated and sustainable solution.

Highlights

The study focuses on a novel sodium-ion-based ferroelectric battery developed at the University of Porto. This battery consists of: (a) a sodium-based ferroelectric solid electrolyte, known for its piezoelectric properties, (b) Zinc (-) and Copper (+) electrodes and (c) a protective layer, made of polymeric shell to prevent moisture absorption and degradation.

The experimental setup includes a vibration testing device (Figure 49), where the battery is attached to an aluminum beam, clamped to an electrodynamic shaker, and subjected to controlled vibrations.

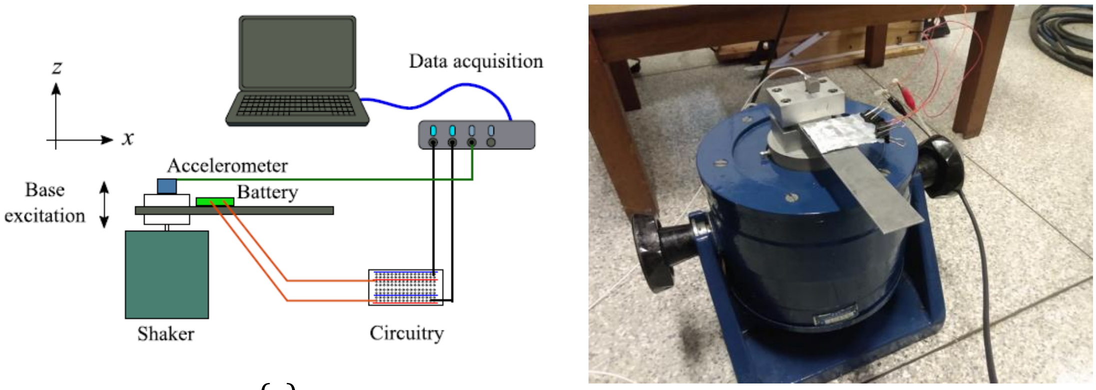

(a)

(b)

Figure 49 - (a) setup of the vibration tests, (b) Depiction of the effective surface area of the battery attached to the aluminum beam mounted to the shaker and accelerometer on the rigid grip.

The battery's electrical response is recorded and analyzed in both time and frequency domains. A Notch filter is applied to reduce electromagnetic interference (particularly 60 Hz noise from the electrical grid). An accelerometer is used to validate the battery's response to vibration-induced strain.

The experimental findings indicate that the sodium-ion-based battery generates an electrical signal at the same frequency as the imposed vibration, confirming its strain-sensing capability. However, the raw signal exhibits strong 60 Hz interference, which can be mitigated using filtering techniques.

Key observations include:

- Accuracy of Strain Sensing: The battery consistently produces a voltage signal corresponding to the vibration frequency, demonstrating its piezoelectric behavior.

- Noise Reduction: The Notch filter significantly improves signal clarity by attenuating 60 Hz interference.

- Sensitivity to Frequency and Amplitude: The battery's response is more pronounced at lower excitation frequencies and higher strain levels. At frequencies above 50 Hz, the response weakens due to reduced beam displacement.

The battery's signal aligns closely with that of the accelerometer, confirming its reliability in detecting structural vibrations. Given its ability to detect mechanical strain, this battery could be integrated into SHM systems to monitor structural integrity in aerospace, automotive, and civil engineering applications.

Despite its promising potential, the sodium-ion-based strain-sensing battery has some limitations: (a) the battery is highly sensitive to 60 Hz noise from the electrical grid, requiring additional filtering techniques, (b) the response weakens at frequencies above 50 Hz, necessitating further optimization of battery design. (c) long-term durability studies are needed to assess how environmental factors affect battery performance over time.

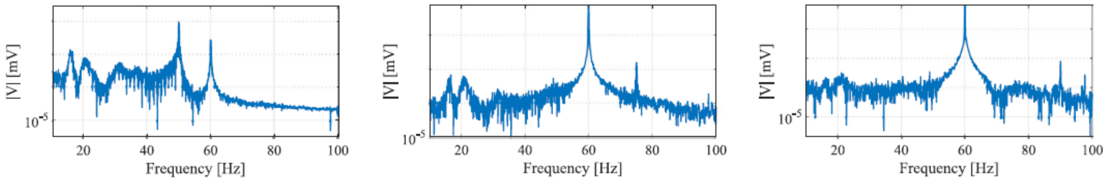

(a)

(b)

(c)

Figure 50 - Battery signal in the frequency domain for frequencies of (a) 50 Hz, (b) 75 Hz, and (c) 90 Hz. In all cases, a mass of 30 g is attached to the tip of the beam tip.

As a conclusion, this study demonstrates that all-solid-state sodium-based batteries can function as strain sensors under vibrational loads. The results highlight their potential for multifunctional applications, particularly in SHM. However, limitations such as susceptibility to electromagnetic interference and reduced sensitivity at higher frequencies need further investigation. Future work will focus on: (a) optimizing battery design to enhance strain sensitivity and reduce noise susceptibility, (b) developing more advanced filtering techniques to improve signal clarity, (c) expanding testing to real-world applications in aerospace, civil engineering, and automotive industries, and (d) investigating long-term durability and reliability in varying environmental conditions.

The findings pave the way for sustainable, self-powered sensing technologies, combining energy storage with structural monitoring. This dual-functionality approach could lead to more efficient, eco-friendly engineering solutions, reducing reliance on separate sensors and power sources, and contributing to the advancement of smart materials and energy-efficient systems.

Sensor Placement Optimization for Composite Aircraft Structures: A Multi-Objective Kriging-Based Approach (UNIFEI - Ref. [18])

Summary:

Structural Health Monitoring (SHM) is a promising means to ensure the safety and longevity of aircraft structures, particularly those made of composite materials. A key challenge in SHM is Sensor Placement Optimization (SPO), which seeks to determine the optimal number and placement of sensors to balance monitoring accuracy and resource efficiency. This study proposes a novel multi-objective optimization methodology integrating Kriging interpolation for mode shape reconstruction and the Lichtenberg Algorithm for sensor placement. The approach aims to minimize the number of sensors while maximizing signal quality and minimizing interpolation error. The methodology is validated using finite element modal analysis data for composite plates and the main rotor blade of an AS-350 helicopter.

Background:

SPO is essential for designing an effective SHM system, as it ensures optimal data collection while reducing costs and complexity. Various SPO methods have been proposed, including genetic algorithms and metaheuristic approaches. However, these methods often struggle to balance the trade-off between the number of sensors and the quality of the collected data.

Kriging is a statistical method originally used in geo-statistics but has proven effective in engineering applications, particularly in mode shape reconstruction. It offers high-accuracy interpolation with fewer sensors, making it an ideal choice for SPO.

The Lichtenberg Algorithm (LA) is a metaheuristic inspired by electrical discharge propagation, which can be used in both single and multi-objective optimization problems. The Multi-Objective Lichtenberg Algorithm (MOLA) efficiently balances different SPO metrics, such as Eigenvector Product (EVP), Fisher Information Matrix (FIM), Effective Independence (EI), Average Driving Point Residue (ADPR), Information Entropy (IE), and Kinetic Energy (KE).

Methodology:

A finite element model (FEM) of the AS-350 main rotor blade was developed using ANSYS Mechanical, employing SHELL281 elements to capture the structure's dynamic behavior (Figure 51). The material properties were determined using inverse modeling techniques. The first six natural vibration modes were extracted, with the second mode excluded due to its negligible modal displacement.

The SPO problem was formulated as a multi-objective optimization problem with the following objectives: (a) minimizing the number of sensors ($F1$), (b) minimizing the interpolation error ($F2$); (c) maximizing signal quality using SPO metrics ($F3$).

MOLA was employed for optimization, with Kriging used for mode shape reconstruction. The Pareto front solutions were analyzed, and the best sensor configurations were selected using the Technique for Order of Preference by Similarity to Ideal Solution (TOPSIS).

(a) Numerical model

(b) Real model

Figure 51 - AS-350 main rotor blade.

A free vibration test was conducted on an AS-350 rotor blade to validate the numerical methodology. Sensors were placed at the optimized positions, and vibration signals were collected using an accelerometer and impact hammer. The experimental results were compared with numerical predictions to evaluate accuracy.

Results and Conclusions:

The Pareto front solutions indicated a trade-off between minimizing sensor count and maximizing data quality. The TOPSIS method identified optimal configurations ranging from 13 to 32 sensors, achieving interpolation errors below 3%. The Information Entropy (IE) metric resulted in the lowest interpolation error (0.82%) with 26 sensors, making it the most balanced solution.

The experimental Frequency Response Functions (FRFs) confirmed the numerical predictions, though some discrepancies were observed due to noise and environmental influences. Kriging-based mode shape reconstruction from experimental data showed inconsistencies, highlighting the need for further improvements in interpolation methods.

The proposed multi-objective optimization approach effectively reduced the number of sensors while maintaining high monitoring accuracy. The integration of MOLA and Kriging provided a reliable method for SPO in composite aircraft structures. Future work should focus on refining interpolation techniques and expanding the methodology to other aerospace applications.

Table 2 - Results of the TOPSIS solution for each optimization.

Metric	F_1	F_2 [%]	Δt [h]
EVP	13	1.5	13
FIM	14	2.6	25
EI	15	1.1	27
ADPR	25	2.1	21
IE	26	0.82	23
KE	32	1.0	14

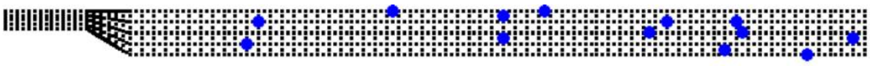

(a) EVP

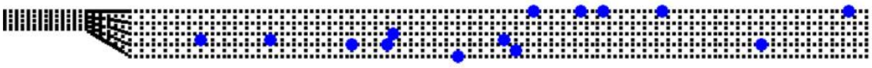

(b) FIM

(c) EI

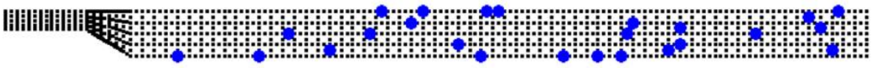

(d) ADPR

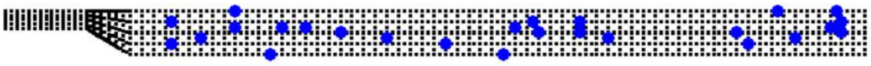

(e) IE

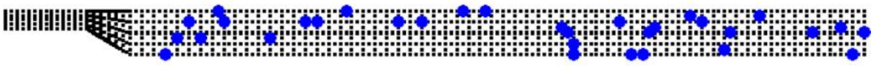

(f) KE

Figure 52 - Sensor arrangement after optimization for each evaluated metric.

Development of Ultrasound for Clamp Monitoring in High-Responsibility Tension Bolted Joints (Embraer)

Summary:

Bolted joints are ubiquitous in engineering structures, playing a critical role in maintaining the structural integrity of various components. The accurate monitoring and maintenance of these joints are essential to prevent catastrophic failures.

A novel project was undertaken to develop an ultrasound-based system for monitoring bolted joints, leveraging advanced techniques to calibrate the ultrasound measurements with tensile tests. This project aimed to provide a reliable, non-invasive method for ensuring the optimal performance of bolted joints in diverse applications.

The primary objective of the project was to create a system that could effectively monitor the preload in bolted joints using ultrasonic waves. The scope included the design and calibration of the system, extensive testing, and validation of its accuracy and reliability. By integrating ultrasound technology, the project aimed to overcome the limitations of traditional monitoring methods, such as visual inspections and torque measurements, which often fall short in precision and efficiency.

Ultrasound technology was chosen due to its proven capability to detect minute changes in material properties and dimensions. In the context of bolted joints, ultrasonic waves can be utilized to measure the elongation of the bolt, which correlates directly with the applied preload. The project employed high-frequency ultrasonic transducers to generate and receive waves that travel through the bolt. By analyzing the time-of-flight and changes in wave characteristics, the system could determine the bolt's elongation with high precision.

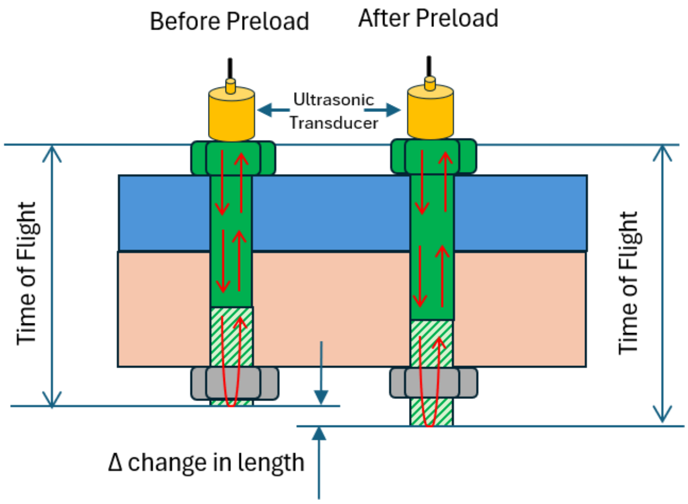

Figure 53 - Ultrasound technology (schematic).

To ensure the accuracy of the ultrasonic measurements, a rigorous calibration process was essential. The project team conducted tensile tests on bolts to establish a reliable relationship between the ultrasonic readings and the actual preload. Tensile tests involve applying a controlled, increasing load to the bolt until a predefined level of tension is reached. During these tests, ultrasonic measurements were taken at various load stages to capture the correlation between bolt elongation and ultrasonic wave propagation.

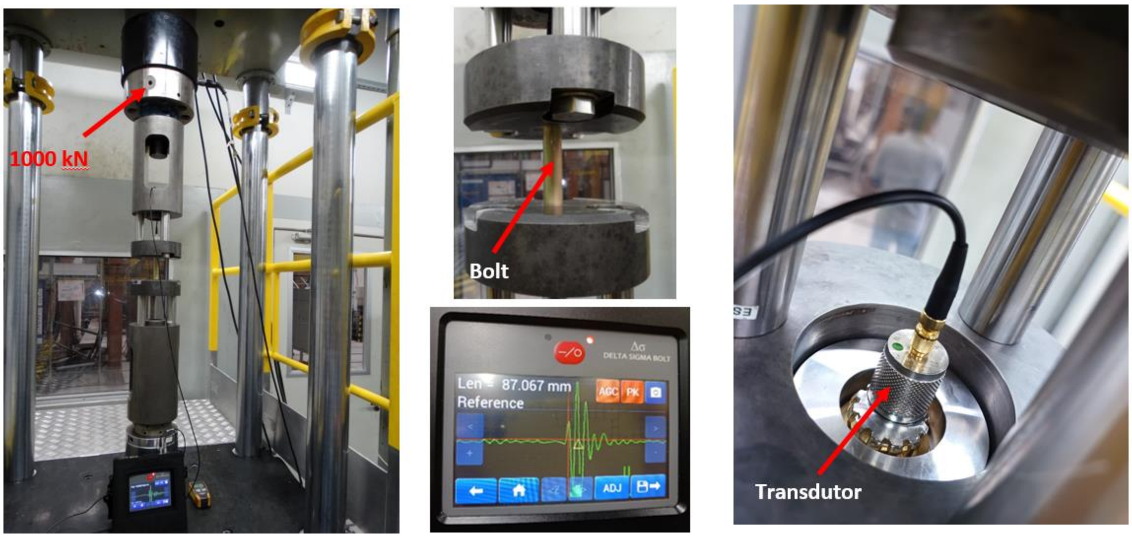

Figure 54 - Tensile test – overview.

The data collected from the tensile tests were used to create a calibration curve, which served as a reference for the ultrasound-based monitoring system. This curve allowed the system to convert ultrasonic readings into precise preload values, ensuring accurate and consistent monitoring.

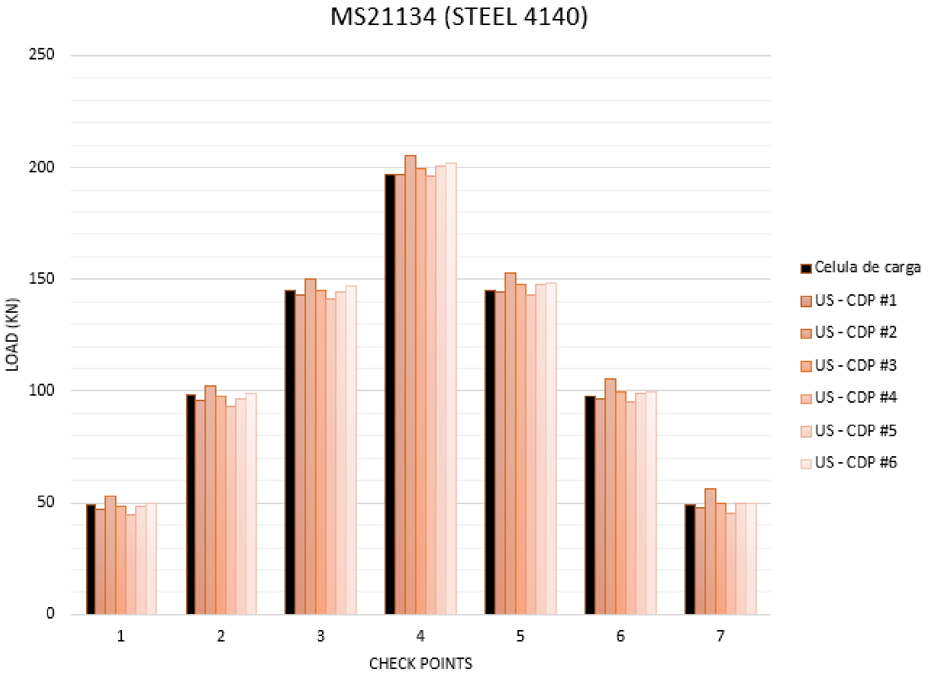

Figure 55 - Calibration plots.

The calibrated system underwent extensive testing in controlled environments to validate its performance. Bolted joints were subjected to various load conditions, and the system's readings were compared against standard measurement techniques. The results demonstrated that the ultrasound-based system provided highly accurate and reliable measurements, with minimal deviation from the actual preload values.

Figure 56 - Calibration standards.

The ultrasound-based bolted joint monitoring system offers several advantages over traditional methods. It is non-invasive, allowing for continuous monitoring without the need for disassembly. Additionally, it provides real-time data, enabling proactive maintenance and early detection of potential issues. The system's precision and reliability make it suitable for applications in critical infrastructure, aerospace, automotive, and industrial machinery.

Looking forward, the project paves the way for further advancements in non-destructive testing and monitoring technologies. The integration of advanced data analytics and machine learning algorithms could enhance the system's capabilities, providing even greater insights into the health and performance of bolted joints.

In conclusion, the development of the ultrasound-based monitoring system represents a significant step forward in the field of structural health monitoring. By combining innovative technology with rigorous calibration and testing, the project has delivered a powerful tool for ensuring the safety and reliability of bolted joints in various engineering applications.

Machine Learning Applied to Crack Detection for Structure Health Monitoring (Embraer)

Summary:

As an important resource in the aeronautical industry, Structural Health Monitoring (SHM) systems are largely employed as crucial element in maintenance and inspection activities, with recent emphasis in extracting the information from the structural responses through Machine Learning (ML). Through Finite Element Analysis (FEA), it is possible to simulate multiple damage scenarios for a certain structure and consequently generate large datasets which can be used for the development of more accurate ML classifiers for damage detection.

The present study uses numerous scenarios generated using FEA to train a Neural Network (NN) that uses strain gauges monitoring on a structure to detect the position of a crack by measuring its strain variation. The number of strain gauges and their location are optimized for better precision and to minimize human resources required, costs and time consumed in practical applications. Different crack scenarios are explored on a representative structural numerical model to study the NN prediction capabilities.

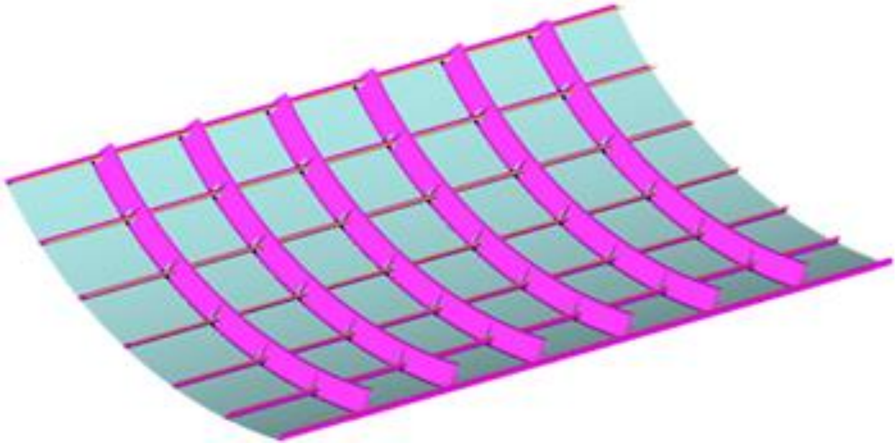

Figure 57 - Finite element model parametric.

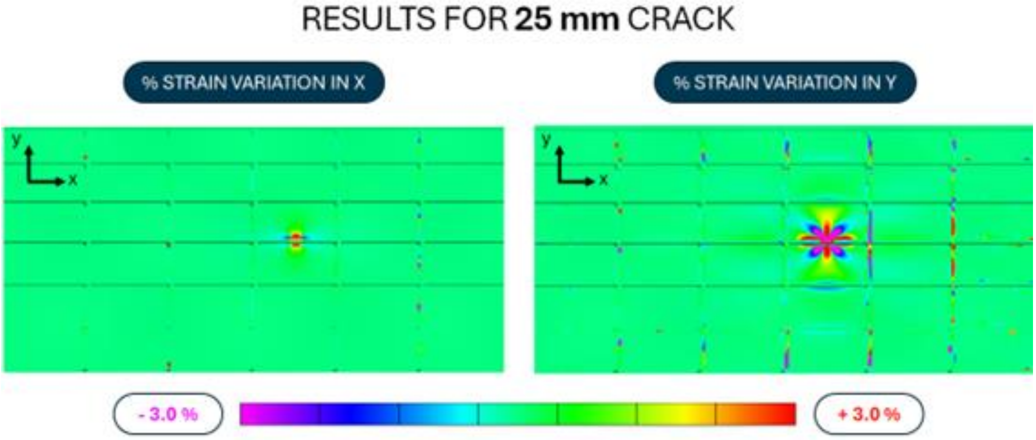

Figure 58 - Strain results in damaged panel.

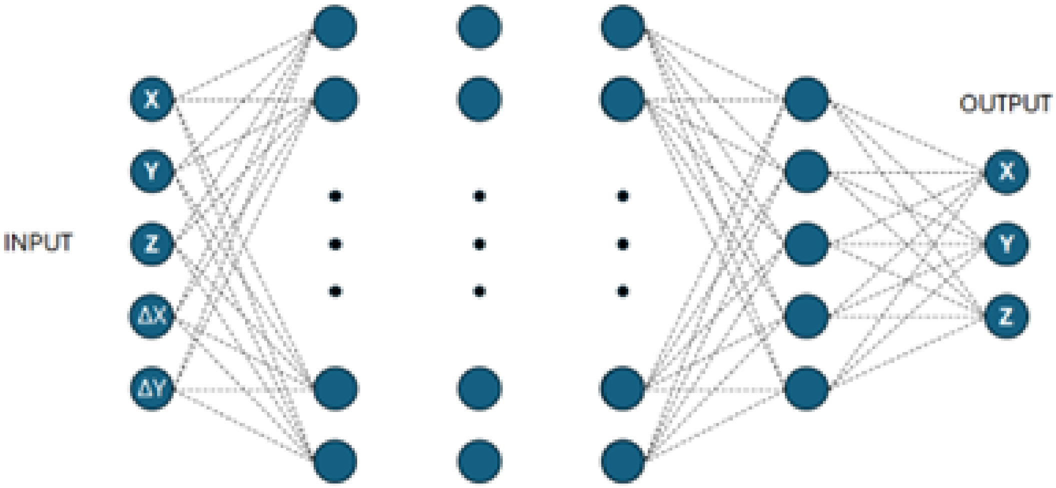

Figure 59 - Neural network architecture – schematic.

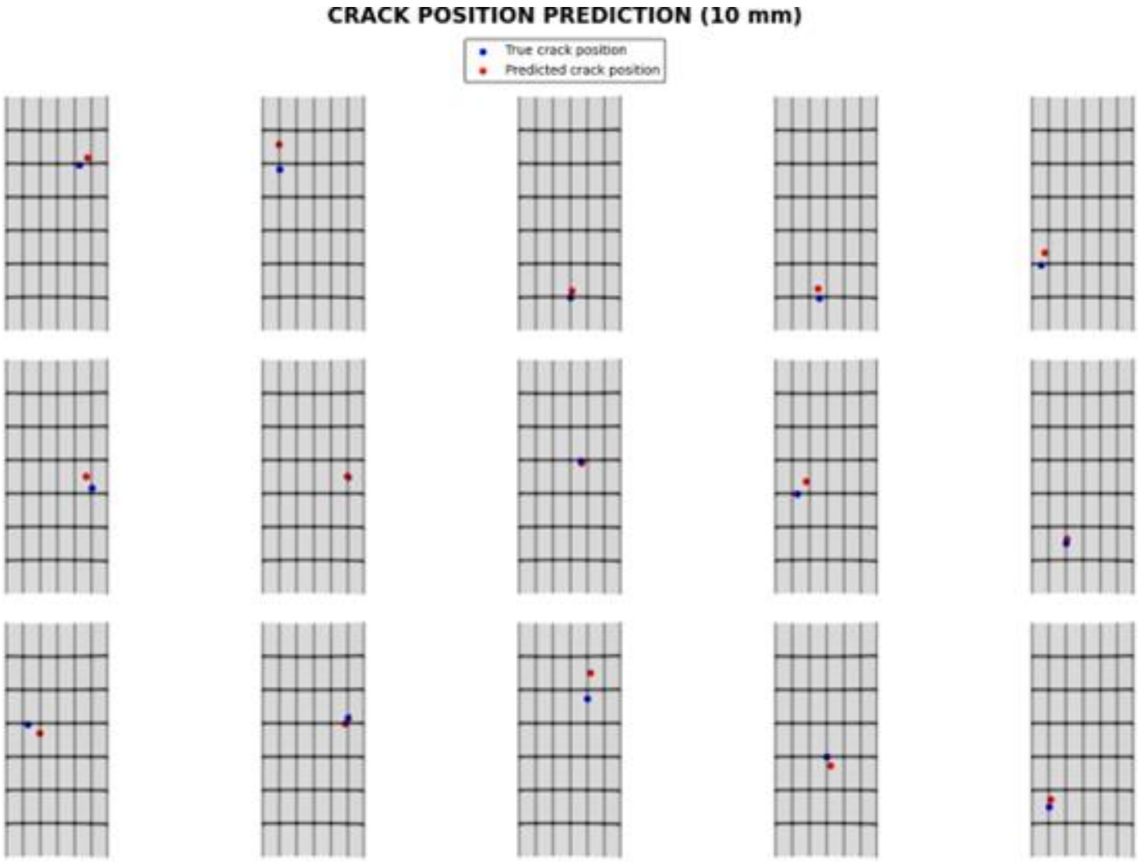

Figure 60 - Example of results correlation.

New Trends of Damage Detection and Identification Based on Vibrothermography in Composite Material (UNIFEI - Ref. [19])

Summary:

The article explores the advancements in using vibrothermography for detecting and identifying damage in composite materials. Vibrothermography combines mechanical vibrations to excite the material and infrared thermography to map the surface temperature, revealing internal damages through temperature variations.

Highlights:

The authors highlight the growing use of composite materials in various industries due to their advantageous properties. The study focuses on the last decade's research trends in vibrothermography, emphasizing damage identification, heat generation mechanisms, and mathematical methods for data post-processing.

Damage Detection: vibrothermography is effective in detecting different types of damage, including barely visible impact damage (BVID), delaminations, notches, flat-bottom holes, and cracks. The technique is particularly useful for identifying BVID, which is challenging to detect visually but can cause significant structural issues. The study reviews various impactors used to generate BVID and other pre-established damages in composite materials, demonstrating the technique's ability to detect these damages.

Understanding heat generation mechanisms is crucial for efficient damage detection. The study discusses two primary mechanisms: viscoelastic heating and Local Defect Resonance (LDR). Viscoelastic heating occurs when high stress concentrations generate heat around the damage during intense vibrations. LDR involves the amplification of local vibrations at a defect's characteristic frequency, resulting in significant temperature variations. The authors present equations and experimental studies to illustrate these mechanisms.

Vibrothermography: the effectiveness of vibrothermography depends on the characteristics of the applied signals. The study highlights the importance of using signals with appropriate frequencies and amplitudes to excite the material efficiently. Multi-harmonic signals, composed of the specimen's natural frequencies, are particularly effective in detecting a wide range of damages. Examples of different signals used in research and their impact on damage detection are provided.

Damage detection can be performed analytically, numerically, experimentally, or through a combination of these methods. Experimental analysis is the most common, involving specific setups to capture thermal images after mechanical excitation. Numerical and analytical methods use equations to model the physical phenomena and generate temperature gradients on the material's surface. The study presents various experimental setups and numerical models used in recent research.

Post-processing of data obtained from vibrothermography tests is essential for improving damage detection efficiency. Techniques like Principal Component Analysis (PCA), Independent Component Analysis (ICA), Fourier Transform (FT), Power Spectral Density (PSD), and Operational Modal Analysis (OMA) are used to enhance the quality of thermal images and extract relevant features. The authors provide examples of these techniques and their applications in recent studies.

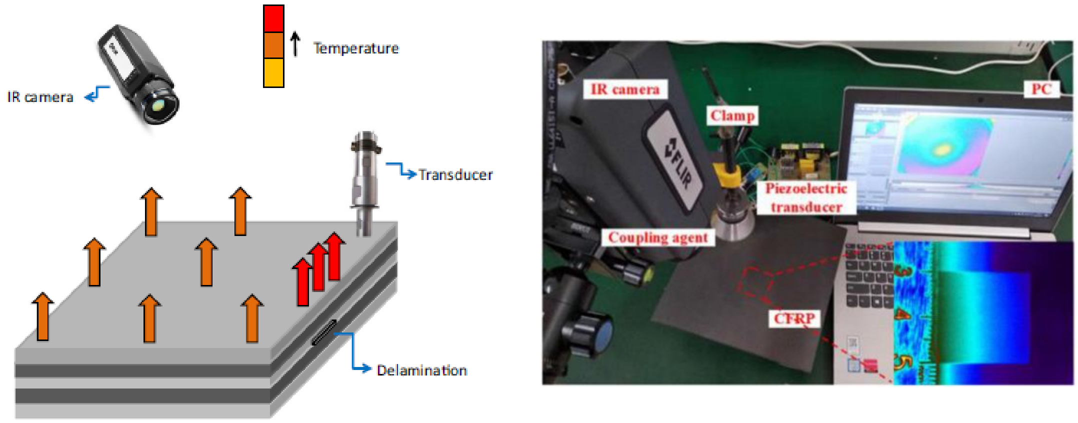

Figure 61 - (a) Schematic illustration of heat generation in damage, (b) example of experimental setup for vibrothermography.

The study concludes that vibrothermography is a valuable technique for detecting and characterizing damage in composite materials. The advancements in infrared cameras, excitation mechanisms, and post-processing methods have significantly improved the technique's efficiency. The authors emphasize the importance of understanding heat generation mechanisms and using appropriate excitation signals to maximize damage detection. They also highlight the role of post-processing techniques in enhancing the quality of thermal images and improving damage characterization.

7. AIRWORTHINESS

E-Jets Widespread Fatigue Damage Compliance Work (Embraer)

Summary:

The WFD Rule (14 CFR 26 Subpart C – Aging Airplane Safety – Widespread Fatigue Damage – Ref. [20]) became effective on January 14, 2011. While Part 26 as a whole is related to Continued Airworthiness and Safety Initiatives, §26.21 is the specific requirement related to WFD. This requirement established a period for Type Certificate Holders (TCH) to: (a) develop a methodology for WFD assessment, (b) develop and submit a compliance plan, and (c) perform the assessment for the applicable aircraft (i.e., with maximum takeoff weight greater than 75,000 pounds), evaluating structures susceptible to WFD and publishing a Limit of Validity (LOV) in the Airworthiness Limitation Section (ALS) of the Instructions of Continued Airworthiness (ICA) for these aircraft. The TCH must demonstrate that the airplane will be free from widespread fatigue damage up to the LOV, as well as identify and develop service actions whenever deemed necessary to preclude WFD up to the LOV. The rule also requires that the operators of the affected airplanes incorporate the LOV and the additional service actions (if necessary) into the maintenance program for that airplane and prohibits the operators of flying an airplane beyond its LOV, unless an extended LOV is approved.

The deadline for Embraer to accomplish with §26.21 requirement was January 14, 2016. During this period, Embraer 170 and 190 aircraft Full-scale Fatigue Tests were successfully completed (after three lifetimes, followed by residual strength tests and teardown inspections) and the majority of the assessment work was performed as planned. However, during the compliance period, Embraer has identified some structures that might need additional maintenance tasks to support the LOV and conducted additional tests and further analysis, either to develop the necessary service actions or to reduce these items, under a schedule agreed with ANAC (the "National Civil Aviation Agency" from Brazil) and the FAA. These additional tasks had to be accomplished during a period of 10 years, the so-called Binding Schedule. Some tasks were later removed from the Binding Schedule, by means of Exemptions, granted by the FAA. Presently, all these additional activities are finished, and the schedule was already accomplished as of June 2025.

In the year 2021, EASA released Part 26 Ageing Aircraft Requirements (Ref. [21]). There are many categories of aircraft affected by this requirement, including families of commercial and executive jets made in Brazil. Most of the requirements present commonality with previous FAA and ANAC Part 26 requirements. Others may require additional documentation for compliance.

This is a long-term work, and some activities may last until 2026 or later, following EASA schedule.

8. REFERENCES

Crack Growth Analysis and Simulation

1. Felipe L. Lopes, Rafael M. Lins, Mariano A. Arbelo, . *Crack propagation analysis due to fatigue using the Stable Generalized Finite Element Method (SGFEM)*, presented in XLV The XLV Ibero-Latin American Congress on Computational Methods in Engineering –(CILAMCE 2024), Maceió, Brazil, November 2024.

2. Felipe L. Lopes, *Application of the Stable Generalized Finite Element Method (SGFEM) for Analysis of Crack Propagation due to Fatigue*, MsC Dissertation, Technological Institute of Aeronautics, 2023.

Metallic Materials - Fretting

3. Raphael. A. Cardoso, Giorgio A. B. Oliveira, Gabriel M. J. Almeida, José. A. Araújo, *A Simple Linear Regression Strategy for Fretting Fatigue Life Estimates*, Tribology International, Vol. 198 (2024), https://doi.org/10.1016/j.triboint.2024.109852

4. Lucas C. Araújo, Lucival Malcher, Déborah de Oliveira, José A. Araújo, *A new multiaxial fatigue endurance model for high strength steels taking into account the presence of small defects*, International Journal of Fatigue, 178 (2024), https://doi.org/10.1016/j.ijfatigue.2023.107981

5. Giorgio A. B. Oliveira, Raphael A. Cardoso, Raimundo C. S. Freire Jr., Thiago Doca, José A. Araújo, *On the generalization capability of artificial neural networks used to estimate fretting fatigue life*, Tribology International, 192 (2024), https://doi.org/10.1016/j.triboint.2023.109222

6. Giorgio A. B. Oliveira, Raphael A. Cardoso, Raimundo C. S. Freire Jr., *A generalized ANN-multiaxial fatigue nonlocal approach to compute fretting fatigue life for aeronautical Al alloys*, Tribology International, 180 (2023), https://doi.org/10.1016/j.triboint.2023.108250

Metallic Materials – Mechanical Processes and Surface Treatments

7. Gabriel Peinado, Cauê Carvalho, Carlos Baptista, *Effects of interrupted aging T6I4 on hardness and fracture toughness of aeronautic AA7050 alloy*, Journal of the Brazilian Society of Mechanical Sciences and Engineering (2024) 46:498 https://doi.org/10.1007/s40430-024-05069-5

Composite Materials

8. J.J. van de Kerk, Rodolfo F. V. De Melo, Giovanni Bastiani, Maurício V. Donadon, Mariano A. Arbelo, *A numerical and experimental study of fasteners as a delamination arrest mechanism in composite laminates under mode I loading*, Thin-Walled Structures 191 (2023), https://doi.org/10.1016/j.tws.2023.111047

9. Francisco M. Monticeli, Felipe R. Fuga, Mariano A. Arbelo, Maurício V. Donadon, *The effect of fibre orientation on fatigue crack propagation in CFRP: Finite fracture mechanics modelling for open-hole configuration*, Engineering Failure Analysis, 161 (2024), https://doi.org/10.1016/j.engfailanal.2024.108278

10. Francisco M. Monticeli, Felipe R. Fuga, Mariano A. Arbelo, Maurício V. Donadon, *Investigation on induced intra/interlaminar damage propagation in CFRP subjected to cyclic tensile loading after impact* (TAI), In: Altenbach, H., Gao, XW., Syngellakis, S., Cheng, A.HD., Lampart, P., Tkachuk, A. (eds) Advances in Mechanical and Power Engineering II. CAMPE 2023. Lecture Notes in Mechanical Engineering. Springer, https://doi.org/10.1007/978-3-031-82979-6_23

11. Denys Marques, Fernando Madureira, Volnei Tita, *Data reduction methods in the fatigue analysis of the Double Cantilever Beam, Part I: Fundaments and virtual fatigue testing*, Composite Structures 324 (2023) https://doi.org/10.1016/j.compstruct.2023.117527

12. Denys Marques, Fernando Madureira, Volnei Tita, *Data reduction methods in the fatigue analysis of the Double Cantilever Beam, Part II: Evaluation and case studies*, Composite Structures 324 (2023), https://doi.org/10.1016/j.compstruct.2023.117528

13. Rafael Beck, Jailto A. P. Da Silva, Lucas F.M. da Silva, Volnei Tita, Ricardo de Medeiros, *Assessing critical fracture energy in Mode I for bonded composite joints: A numerical-experimental approach with uncertainty analysis*, Proceedings of the Institution of Mechanical Engineers, Part L: Journal of Materials: Design and Applications. 2024; doi:10.1177/14644207241229601

14. Felipe R. Fuga, *Progressive intralaminar damage in woven composite materials under mixed-mode fracture*, PhD Thesis, Technological Institute of Aeronautics, 2024.

15. G. H. M. Oliveira, Sergio T. Amancio-Filho, L. B. Canto, *Processing understanding, mechanical durability and hygrothermal stability of PC/AA6061 hybrid joints produced via injection overmolding*, International Journal of Adhesion & Adhesives 130 (2024), https://doi.org/10.1016/j.ijadhadh.2023.103617

Structural Health Monitoring

16. Bruno G Christoff , Denys Marques, João P. Carmo, Maria H. Braga, Volnei Tita, On the strain-sensing capabilities of a novel all-solid-state sodium-based-electrolyte battery under vibration loads, Mechanical Systems and Signal Processing 215 (2024), https://doi.org/10.1016/j.ymssp.2024.111390

17. Bruno G Christoff , Denys Marques, Maísa M. Maciel, Pouria Ataabadi, João Carmo, Maria H. Braga, Rui M. Guedes, Marcílio Alves and Volnei Tita, *Response of a novel all-solid-state sodium-based-electrolyte battery to quasi-static and*

dynamic stimuli, Proceedings of the Institution of Mechanical Engineers Part L Journal of Materials Design and Applications
https://doi:10.1177/14644207241247732

18. Felipe M. S. Mello, Guilherme F. Gomes, Sensor placement optimization for composite aircraft structures: A multi-objective Kriging-based approach, Composite Structures, 353 (2025)
https://doi.org/10.1016/j.compstruct.2024.118723

19. Lucas A. de Oliveira, Guilherme F. Gomes, João L. J. Pereira, Matheus B. Francisco, Anthonin Demarbaix, Sebastião S. Cunha, *New Trends of Damage Detection and Identification Based on Vibrothermography in Composite Material,* Journal of Nondestructive Evaluation 42, 57 (2023)
https://doi.org/10.1007/s10921-023-00963-9

Airworthiness

20. https://www.ecfr.gov/current/title-14/chapter-I/subchapter-C/part-26

21. EASA (European Aviation Safety Agency) – CS-26 requirement and AMC 20-20,
https://www.easa.europa.eu/en/downloads/121014/en

https://www.easa.europa.eu/en/downloads/121020/en